CHAPTER 2 LITERATURE REVIEW

2.1 Introduction

Due to largely increasing in the traffic volume and truck load, many asphaltic concrete pavements in Thailand are susceptible to damages. These damages include rutting and cracking of pavement which are the main problems. A high performance pavement is required to solve this problem. In addition, the realistic behavior is important for model of pavement because the strength and deformation behaviors of asphaltic concrete are often assumed isotropic which is not realistic.

2.2 Theory of elasticity

2.2.1 Isotropic elasticity

Elastic, recoverable, material response is easier to describe and comprehend than plastic, irrecoverable response. Some essential elements of the theory of elasticity will be presented in this section.

A familiar introduction to the elastic properties of materials is obtained by the simple experimental procedure of hanging weights on a wire and measuring the elongation (Fig. 2.1a). For many materials, there is a range of loads for which the elongation varies linearly with the applied load P (Fig. 2.1b) and is recovered when the load is removed. There is no permanent deformation of the wire.

The slope of the linear relationship is related to the unconfined uniaxial stiffness of the material of the wire. Young's modulus E is expressed as

$$E = \frac{P / A}{\delta l / l} \tag{2.1}$$

where P is the load on the wire of area A and length l, and δl is the extension of the wire.

The experimental introduction to elasticity is usually restricted to observation of the load: extension properties of tensile specimens. However, if a micrometer were available to measure the changing diameter d of the wire, then one would observe that, as the wire becomes longer, its diameter becomes smaller (Figs. 2.1c and 2.2a). The ratio of the magnitude of the induced diametral strain to the imposed longitudinal strain is Poisson's ratio ν:

$$\nu = \frac{-\delta d / d}{\delta l / l} \tag{2.2}$$

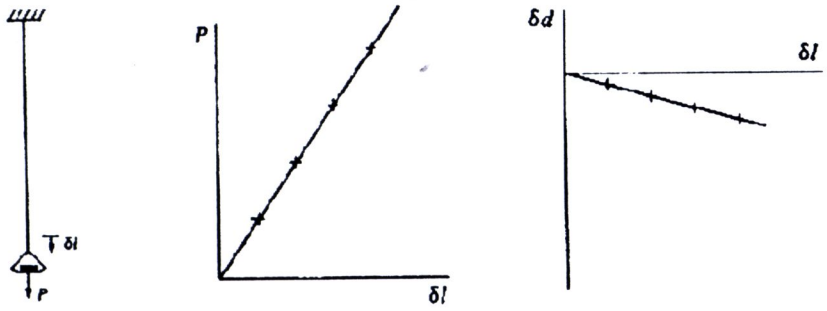

Figure 2.1 Tensile test on metal wire: (a) test arrangement; (b) load-extension relationship; and (c) changes in diameter with length (Wood, 1990)

It is well known that the pair of constants E and ν is sufficient to describe the elastic response of isotropic materials. These two constants are probably the most easily understood elastic constants because direct experimental observation of them is so straightforward. However, in many ways it is more fundamental to use an alternative pair of elastic constants: the bulk modulus K and shear modulus G, which divide the elastic deformation into a volumetric part (change of size at constant shape, Fig. 2.2b) and a distortional part (change of shape at constant volume, Fig. 2.2c), respectively.

The benefit of using K and G is particularly great when elasticity of soils is considered. Undrained deformation of soils is specifically concerned with deformation of soil at constant volume, that is, pure distortion of soil, a change of shape without change in size. The distinction between undrained and drained processes is only relevant because there are some processes (in general, inelastic ones) during which soil express a desire to change in size as well as shape as they are sheared.

The relationships between the two sets of constants can be deduced by considering the change in volume of the wire as it is extended, which shows that the bulk modulus K is

$$K = \frac{E}{3(1-2\nu)} \tag{2.3}$$

and by considering the change of the right angle between rays drawn in the material of the wire at $\pm\pi/4$ to the axis of the wire (Fig. 2.2c), which shows that the shear modulus G is:

$$G = \frac{E}{2(1+\nu)} \tag{2.4}$$

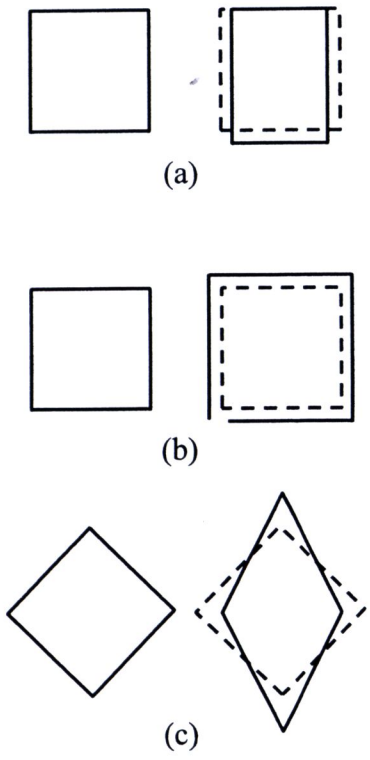

Figure 2.2 (a) Young's modulus describing change in length and Poisson's ratio describing change in width; (b) bulk modulus describing change in size at constant shape; (c) shear modulus describing change in shape at constant volume (Wood, 1990)

2.2.2 Soil elasticity

Unconfined tensile tests on soils are not usually feasible. Compression tests are more commonly performed using the triaxial apparatus and with some lateral confinement provided by the cell pressure. The results of a typical drained test on a soil sample might resemble those shown in Fig. 2.3. This is a conventional triaxial compression test in which the axial stress (or deviator stress) is increased while the lateral stress (or cell pressure) is held constant. The initial linear sections of the stress: strain curve (Fig. 2.3a) (deviator stress q plotted against triaxial shear strain ε_q) and of the volume-change curve (Fig. 2.3b) (volumetric strain ε_p plotted against triaxial shear strain ε_q) might be interpreted as the elastic response of the soil to the imposed changes of stress. Thus, the values of the elastic constants could be deduced.

Young's modulus and Poisson's ratio, can describe the response of a soil specimen to a general triaxial change of effective stress by these equations:

$$\begin{bmatrix} \delta\varepsilon_a \\ \delta\varepsilon_r \end{bmatrix} = \frac{1}{E'} \begin{bmatrix} 1 & -2\nu' \\ -\nu' & 1-\nu' \end{bmatrix} \begin{bmatrix} \delta\sigma'_a \\ \delta\sigma'_r \end{bmatrix} \tag{2.5}$$

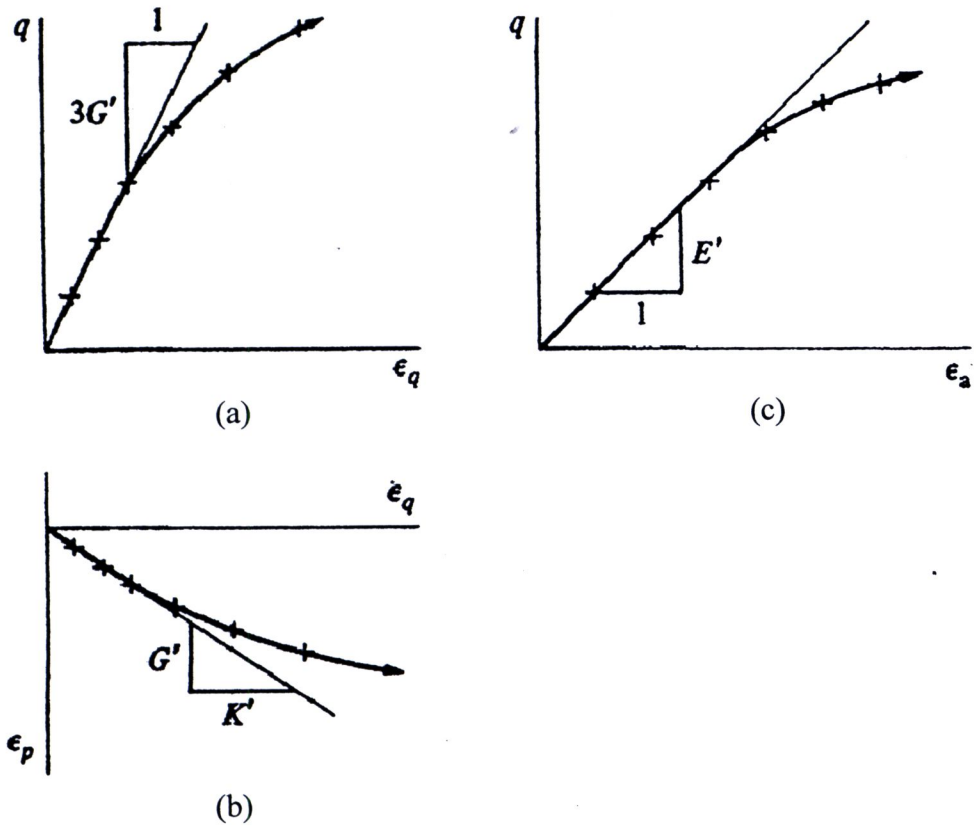

Figure 2.3 Elastic constant deduced from conventional drained triaxial compression test: (a) deviator stress q and triaxial shear strain ε_q; (b) volumetric strain ε_p and triaxial shear strain ε_q; and (c) deviator stress q and axial strain ε_a (Wood, 1990)

For description and analysis of triaxial tests, the mean effective stress p' and deviator stress q are:

$$\begin{bmatrix} p' \\ q \end{bmatrix} = \begin{bmatrix} 1/3 & 2/3 \\ 1 & -1 \end{bmatrix} \begin{bmatrix} \sigma'_a \\ \sigma'_r \end{bmatrix} \tag{2.6}$$

and the increments of volumetric strain $\delta\varepsilon_p$ and triaxial shear strain $\delta\varepsilon_q$ are:

$$\begin{bmatrix} \delta\varepsilon_p \\ \delta\varepsilon_q \end{bmatrix} = \begin{bmatrix} 1 & 2 \\ 2/3 & -2/3 \end{bmatrix} \begin{bmatrix} \delta\varepsilon_a \\ \delta\varepsilon_r \end{bmatrix} \tag{2.7}$$

The elastic response in Eq. 2.5 can then be written more elegantly using bulk modulus and shear modulus to separate effects of changing size and changing shape:

$$\begin{bmatrix} \delta\varepsilon_p \\ \delta\varepsilon_q \end{bmatrix} = \begin{bmatrix} 1/K' & 0 \\ 0 & 1/3G' \end{bmatrix} \begin{bmatrix} \delta p' \\ \delta q \end{bmatrix} \tag{2.8}$$

The off-diagonal zeroes in Eq. 2.8 indicate the absence of coupling between volumetric and distortional effects for this isotropic elastic material. Change in mean stress p' produces no distortion $\delta\varepsilon_q$, and change in the distortional deviator stress q produces no change in volume. The initial gradient of the stress: strain curve in Fig. 2.3a is then $3G'$. The initial gradient of the volume change curve in Fig. 2.3b is

$$\frac{\delta\varepsilon_p}{\delta\varepsilon_q} = \frac{3G'}{K'}\frac{\delta p'}{\delta q} \tag{2.9}$$

For a conventional drained triaxial compression test on a soil specimen, in which we can obtain:

$$\delta q = 3\delta p' \tag{2.10}$$

combining Eq. 2.9 and 2.10, they become:

$$\frac{\delta\varepsilon_p}{\delta\varepsilon_q} = \frac{G'}{K'} \tag{2.11}$$

and the elastic properties have been recovered. Evidently, values of Young's modulus and Poisson's ratio could be deduced using Eq. 2.3 and 2.4.

If drainage from the triaxial sample is prevented, then undrained constant volume response is observed. The initial response or the soil specimen may still be elastic, but now, with volume change prevented, pore pressures develop. The response of the soil can be depicted in plot of deviator stress and pore pressure against triaxial shear strain (Fig. 2.4). The imposition of a condition of constant volume on Eq. 2.8 implies that

$$\frac{\delta p'}{K'} = 0 \tag{2.12}$$

which requires either that

$$K' = \infty$$

or

$$\delta p' = 0$$

There is no reason why the bulk modulus of the soil skeleton should be infinite; certainly the act of closing the drainage tap on the triaxial apparatus can have no influence on the elastic properties of the soil skeleton. Consequently, the only reasonable solution to Eq. 2.12 is:

$$\delta p' = 0 \tag{2.13}$$

The pore pressure changes reflect directly the imposed changes in total mean stress as:

$$\delta u = \delta p \tag{2.14}$$

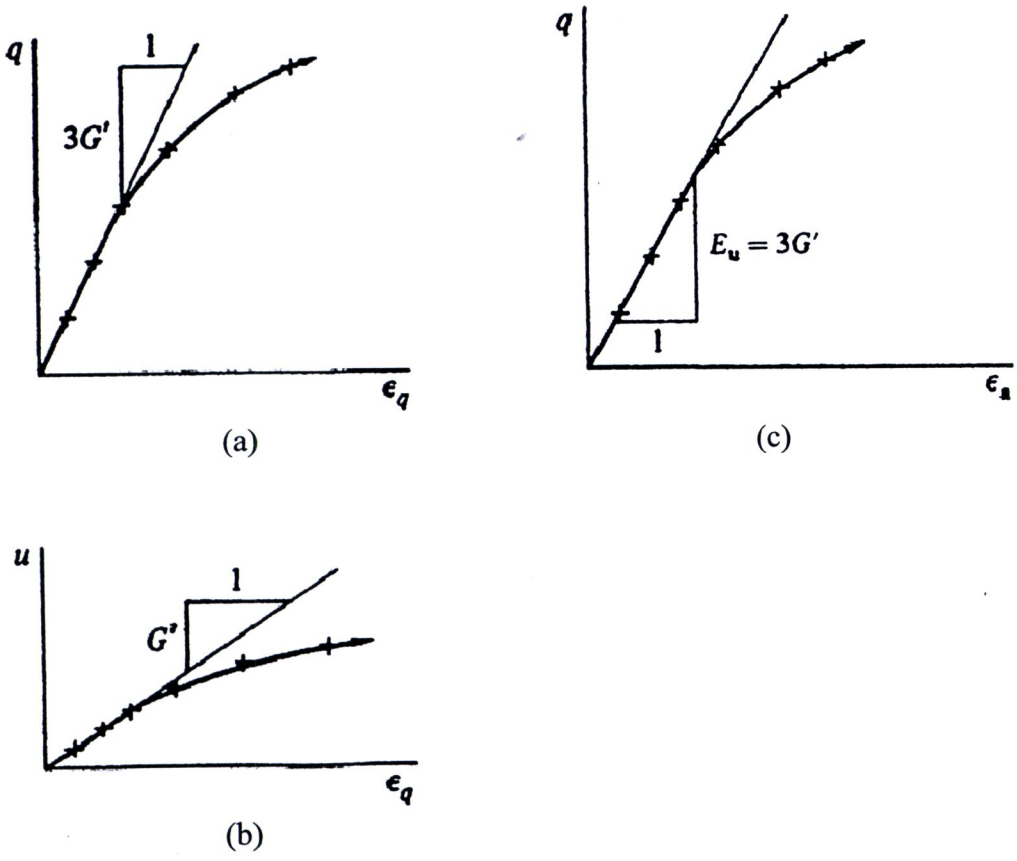

Figure 2.4 Elastic constant deduced from conventional undrained triaxial compression test: (a) deviator stress q and triaxial shear strain ε_q; (b) pore pressure u and triaxial shear strain ε_q; and (c) deviator stress q and axial strain ε_a (Wood, 1990)

and, irrespective of the total stress path, the effective stress path is vertical in the p':q plane *(AB* in Fig. 2.5a). Evidently, *any* total stress path could be imposed; if one of these paths had no applied change in total mean stress, $\delta p = 0$, then the soil would have no desire to change in volume under the purely distortional stress changes and hence no tendency to generate any pore pressure.

The constant volume condition imposes no constraint on the change in *shape* of the soil sample, and Eq. 2.8 makes it clear that the slope of the deviator stress: triaxial shear strain plot (Fig. 2.4a) will again be $3G'$, as in the drained test. For a conventional undrained triaxial compression test in which the cell pressure is held constant while the axial stress is increased, we obtain:

$$\delta p = \frac{\delta q}{3} = \delta u \tag{2.15}$$

and the slope of the plot of pore pressure against triaxial shear strain (Fig. 2.4b) is G'. If at some stage of the undrained loading, the drainage tap is opened and the pore pressure

is allowed to dissipate at constant total stresses, then some deformation of the soil will occur. With the total stresses constant, the deviator stress $q = \sigma'_a - \sigma'_r = \sigma_a - \sigma_r$ cannot change, and the effective stress path for this dissipation process is parallel to the p' axis (BC in Fig. 2.5a). It is then apparent from Eq. 2.8 that the accompanying deformation will involve only change of size ($\delta\varepsilon_p > 0$) with no change in shape ($\delta\varepsilon_q = 0$).

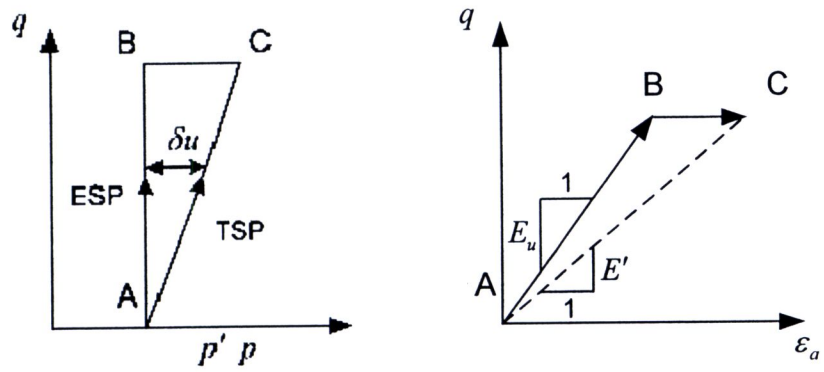

Figure 2.5 Undrained shearing AB and subsequent pore pressure dissipation BC in conventional triaxial compression test: (a) total and effective stress paths; and (b) deviator stress q and axial strain ε_a (Wood, 1990)

Although the behavior of soil elements is controlled by changes in effective stresses, it is often useful to describe the elastic response of soil in terms of changes in total stresses. Equilibrium equations for a soil continuum can be written in terms of total stresses without having to introduce pore pressures, and analytical procedures may often lead more readily to distributions of total stresses than to distributions of effective stress. The observed response of a soil element must, however, be identical whether it is treated in terms of total stresses or effective stresses.

The total stress equivalent of Eq. 2.8 is:

$$\begin{bmatrix} \delta\varepsilon_p \\ \delta\varepsilon_q \end{bmatrix} = \begin{bmatrix} 1/K_u & 0 \\ 0 & 1/3G_u \end{bmatrix} \begin{bmatrix} \delta p \\ \delta q \end{bmatrix} \tag{2.16}$$

The distinction between elastic properties in terms of total or effective is only helpful for constant volume undrained conditions; this is the reason for the subscript u on the bulk modulus and shear modulus in Eq. 2.16.

For an undrained constant volume condition, $\delta\varepsilon_p = 0$ implies that:

$$\frac{\delta p}{K_u} = 0 \tag{2.17}$$

where the effective stress description of Eq. 2.8 and 2.12 looks at the triaxial soil sample from inside the membrane, the total stress description of Eq. 2.16 and 2.17 looks at the sample from outside the membrane. There can now be no constraint on the total stress path that is imposed. The condition of no volume change must emerge whatever the externally applied changes in total stress. Hence, the total stress undrained bulk modulus K_u must be infinite,

$$K_u = \infty \tag{2.18}$$

This, from the general equation Eq. 2.3, implies that the undrained Poisson's ratio is

$$\nu_u = \frac{1}{2} \tag{2.19}$$

The deviator stress q is not affected by drainage conditions because, as a difference of two stresses, it is independent of pore pressure. The shearing, or change of shape, of the soil $\delta\varepsilon_q$ calculated from Eq. 2.8 and 2.16 must be identical and hence:

$$G_u = G' \tag{2.20}$$

and the shear modulus is independent of the drainage conditions.

Given the link between shear modulus, Young's modulus, and Poisson's ratio implied by Eq. 2.4 the undrained and drained values of Young's modulus, E_u and E', respectively, are not independent. From Eq. 2.4 and 2.20, we obtain:

$$\frac{E_u}{2(1+\nu_u)} = \frac{E'}{2(1+\nu')}$$

And then with Eq.2.19, we further obtain:

$$E_u = \frac{3E'}{2(1+\nu')} \tag{2.21}$$

Young's modulus describes the slope of the axial stress: axial strain relationship. In conventional triaxial compression tests in which $\delta\sigma_a = \delta q$, and Young's modulus is the slope of the deviator stress: axial strain relationship. Different slopes, in the ratio given by Eq. 2.21, will be seen in drained and undrained tests (Figs. 2.3c and 2.4c). The effect of allowing drainage to occur after some increments of undrained loading (effective stress path *BC* after *AB* in Fig. 2.5a) is to take the deviator stress: axial strain state from the undrained to the drained line, as shown in Fig. 2.5b.

In summary, for isotropic elastic soil, there are only two independent elastic soil constants. Elastic constants to describe the behavior of soil under special conditions (e.g., in terms of total stresses for undrained conditions) can be deduced from the more fundamental effective stress constants and cannot be chosen independently.

2.2.3 Anisotropic elasticity

Many soils have been deposited over areas of large lateral extent, and the deformations they have experienced during and after deposition have been essentially one-dimensional. Soil particles have moved vertically downwards (and possibly also upwards) with, from symmetry, no tendency to move laterally. The anisotropic elastic properties of the soil reflect this history. The soil may respond differently if it is pushed in vertical or horizontal directions, but it will respond in the same way if it is pushed in any horizontal direction. For example, cylindrical sample *A* in Fig 2.6, taken from the ground with its axis vertical, behaves differently from samples *B, C, D,* and *E*, which have been taken-from the ground with their axes in various horizontal directions; but samples *B, C, D,* and *E* all behave identical.

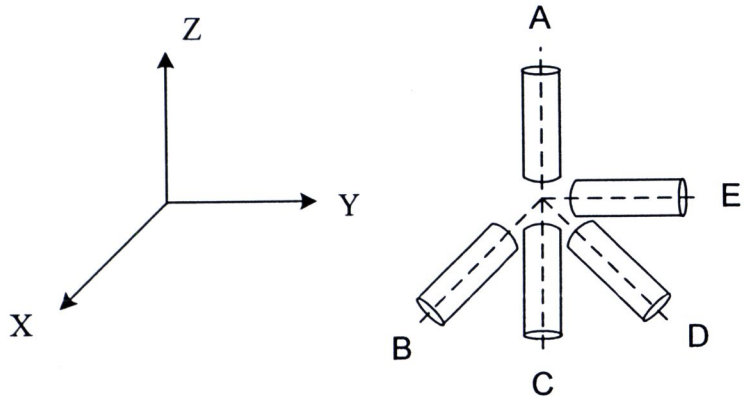

Figure 2.6 Cylindrical soils samples taken out of the ground with their axes vertical (*A*) and horizontal (*B, C, D, E*) (Wood, 1990)

The special form of anisotropy, known as *transverse isotropy* or *cross anisotropy,* requires only five elastic constants for its specification. The form of the relationship between stress increments and strain increments is:

$$\begin{bmatrix} \delta\varepsilon_{xx} \\ \delta\varepsilon_{yy} \\ \delta\varepsilon_{zz} \\ \delta\gamma_{yz} \\ \delta\gamma_{zx} \\ \delta\gamma_{xy} \end{bmatrix} = \begin{bmatrix} \frac{1}{E_h} & \frac{-\nu_{hh}}{E_h} & \frac{-\nu_{vh}}{E_v} & 0 & 0 & 0 \\ \frac{-\nu_{hh}}{E_h} & \frac{1}{E_h} & \frac{-\nu_{vh}}{E_v} & 0 & 0 & 0 \\ \frac{-\nu_{hv}}{E_h} & \frac{-\nu_{hv}}{E_h} & \frac{1}{E_v} & 0 & 0 & 0 \\ 0 & 0 & 0 & \frac{1}{G_{vh}} & 0 & 0 \\ 0 & 0 & 0 & 0 & \frac{1}{G_{vh}} & 0 \\ 0 & 0 & 0 & 0 & 0 & \frac{2(1+\nu_{hh})}{E_h} \end{bmatrix} \begin{bmatrix} \delta\sigma'_{xx} \\ \delta\sigma'_{yy} \\ \delta\sigma'_{zz} \\ \delta\tau_{yz} \\ \delta\tau_{zx} \\ \delta\tau_{xy} \end{bmatrix} \tag{2.22}$$

where the stress and strain increments are referred to rectangular Cartesian axes x, y, and z with the z axis vertical (Fig. 2.6)

Most of the routine soil tests that are performed in practice are triaxial compression tests on samples such as *A* in Fig. 2.6, taken out of the ground which their axes vertical, for example, from some sorts of borehole. Graham and Houlsby (1983) show that it is not possible from such tests to recover three elastic constants for the soil; since two constants are needed for the description of isotropic elastic response, that leaves only one constant through which some anisotropy can be incorporated. They propose a particular form of one-parameter anisotropy which allows certain analytical advantages and leads to a particular form of stiffness matrix relating stress increments and strain increments:

$$\begin{bmatrix} \delta\varepsilon_{xx} \\ \delta\varepsilon_{yy} \\ \delta\varepsilon_{zz} \\ \delta\gamma_{yz} \\ \delta\gamma_{zx} \\ \delta\gamma_{xy} \end{bmatrix} = \frac{1}{E^*} \begin{bmatrix} \frac{1}{\alpha^2} & \frac{-\nu^*}{\alpha^2} & \frac{-\nu^*}{\alpha} & 0 & 0 & 0 \\ \frac{-\nu^*}{\alpha^2} & \frac{1}{\alpha^2} & \frac{-\nu^*}{\alpha} & 0 & 0 & 0 \\ \frac{-\nu^*}{\alpha} & \frac{-\nu^*}{\alpha} & 1 & 0 & 0 & 0 \\ 0 & 0 & 0 & \frac{2(1-\nu^*)}{\alpha} & 0 & 0 \\ 0 & 0 & 0 & 0 & \frac{2(1-\nu^*)}{\alpha} & 0 \\ 0 & 0 & 0 & 0 & 0 & \frac{2(1-\nu^*)}{\alpha^2} \end{bmatrix} \begin{bmatrix} \delta\sigma'_{xx} \\ \delta\sigma'_{yy} \\ \delta\sigma'_{zz} \\ \delta\tau_{yz} \\ \delta\tau_{zx} \\ \delta\tau_{xy} \end{bmatrix} \tag{2.23}$$

In these expressions, E^* and ν^* represent modified values of Young's modulus and Poisson's ratio for the soil, and α. is the anisotropy parameter. Equation 2.23 can be compared with the completely general five-constant description of transverse isotropy. Equations 2.22-2.23 give the complete stiffness and compliance matrices which are necessary for any analysis of transversely isotropic elastic soil. However, to interpret the results of triaxial tests, it is helpful once again to look at description of changes in size and in shape. Still following Graham and Houlsby (1983), one finds the stiffness equation to be:

$$\begin{bmatrix} \delta p' \\ \delta q \end{bmatrix} = \begin{bmatrix} K^* & -J \\ -J & 3G^* \end{bmatrix} \begin{bmatrix} \delta\varepsilon_p \\ \delta\varepsilon_q \end{bmatrix} \tag{2.24}$$

where K^* and G* are modified values of bulk modulus and shear modulus, and the presence of the two off-diagonal terms J shows that there is now some cross-coupling between volumetric and distortional effects. The quantities K^*, G^*, and J can be expressed in terms of the quantities E^*, ν^*, and α from Eq. 2.23 as:

$$K^* = \frac{E^*(1-\nu^*+4\alpha\nu^*+2\alpha^2)}{9(1+\nu^*)(1-2\nu^*)} \tag{2.25}$$

$$G^* = \frac{E^*(2-2\nu^*-4\alpha\nu^*+\alpha^2)}{6(1+\nu^*)(1-2\nu^*)} \tag{2.26}$$

$$J = \frac{E^*(1-\nu^*+\alpha\nu^*-\alpha^2)}{3(1+\nu^*)(1-2\nu^*)} \tag{2.27}$$

It may be confirmed that for $\alpha = 1$, these expressions for K^* and G^* reduce to Eq. 2.3 and 2.4 and that $J = 0$. The compliance form of Eq. 2.24 is

$$\begin{bmatrix} \delta\varepsilon_p \\ \delta\varepsilon_q \end{bmatrix} = \frac{1}{D}\begin{bmatrix} 3G^* & -J \\ -J & K^* \end{bmatrix}\begin{bmatrix} \delta p' \\ \delta q \end{bmatrix} \tag{2.28}$$

with

$$D = 3K^*G^* - J^2 \tag{2.29}$$

The coupling between volumetric and distortional effects implies that constant volume effective stress paths are no longer vertical constant p' paths in the p': q plane [Eq. 2.13 and Fig. 2.5a]. The direction of the path will depend on the value of α. With $\alpha > 1$ the soil is stiffer horizontally than vertically, and the undrained effective stress path shows a decrease in p' (Fig. 2.7). With $\alpha < 1$ the soil is stiffer vertically, and the undrained effective stress path shows an increase in p' (Fig. 2.7). The pore pressure that is observed in an undrained test will be different from the change in total mean stress, with the difference depending on α and ν^*. The direction of the effective stress path is, from Eq. 2.28:

$$\frac{\delta q}{\delta p} = \frac{3G^*}{J} \tag{2.30}$$

or

$$\frac{\delta q}{\delta p'} = \frac{3(2-2\nu^*-4\alpha\nu^*+\alpha^2)}{2(1-\nu^*+\alpha\nu^*-\alpha^2)} \tag{2.31}$$

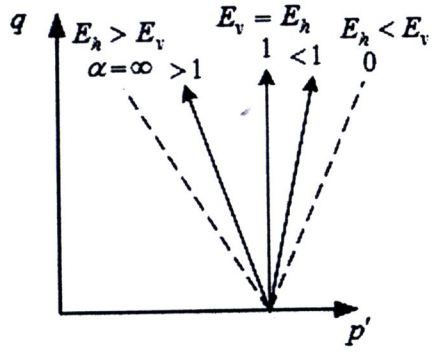

Figure 2.7 Effective stress paths for constant volume deformation of cross-anisotropic elastic soil (Wood, 1990)

The coupling between change of size and change of shape also implies that shear strains will occur along stress paths in which q is held constant, for example, isotropic compression $q = 0$ (Fig. 2.8). For such a path, from Eq. 2.24,

$$\frac{\delta\varepsilon_q}{\delta\varepsilon_p} = \frac{-J}{3G^*} \tag{2.32}$$

or

$$\frac{\delta\varepsilon_q}{\delta\varepsilon_p} = \frac{-2(1-\nu^*+\alpha\nu^*-\alpha^2)}{3(2-2\nu^*-4\alpha\nu^*+\alpha^2)} \tag{2.33}$$

and the path of this isotropic compression will not in general lie along the $\delta\varepsilon_p$ axis $(\varepsilon_q = 0)$ in the $\varepsilon_p : \varepsilon_q$ strain plane. This ratio (i.e., Eq. 2.33) has limiting values of 2/3 and -1/3 for α very large and very small. These limiting values correspond to compression at constant radial strain $(\delta\varepsilon_r = 0)$ and constant axial strain $(\delta\varepsilon_a = 0)$, respectively.

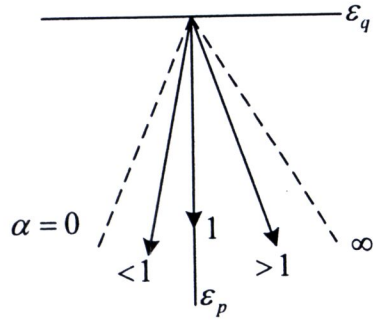

Figure 2.8 Volumetric strain: triaxial shear strain path for compression of cross-anisotropic elastic soil under isotropic stresses (Wood, 1990)

2.3 Anisotropic behavior of geomaterials

The discussion in previous section of soil behavior has been restricted to the theoretical of isotropic and anisotropic elasticity of soil but, in fact, soil behavior is anisotropic. Elastic deformation characteristics of geomaterials are essential part in soil dynamics. However, their possible anisotropy is not well understood. It can be classified into the following three categories;

a) Inherent anisotropic produced when deposited in air or under water or compacted
b) Stress state-induced anisotropy produced by anisotropic stress state
c) Strain history-induced anisotropy produced by large shear (monotonic or cyclic) strain in a certain direction.

Most granular materials deposited naturally or artificially, or compacted vertically, exhibit cross-anisotropic deformation properties, which are symmetrical about the vertical axis. Cross-anisotropy requires only six elastic parameters for the characterization of soil properties (Hoque and Tatsuoka, 1998). The incremental relationship between stresses and strains (Hooke's law) is:

$$\begin{bmatrix} \delta\varepsilon_{xx} \\ \delta\varepsilon_{yy} \\ \delta\varepsilon_{zz} \\ \delta\varepsilon_{yz} \\ \delta\varepsilon_{zx} \\ \delta\varepsilon_{xy} \end{bmatrix} = \begin{bmatrix} \frac{1}{E_h} & \frac{-\nu_{hh}}{E_h} & \frac{-\nu_{vh}}{E_v} & 0 & 0 & 0 \\ \frac{-\nu_{hh}}{E_h} & \frac{1}{E_h} & \frac{-\nu_{vh}}{E_v} & 0 & 0 & 0 \\ \frac{-\nu_{hv}}{E_h} & \frac{-\nu_{hv}}{E_h} & \frac{1}{E_v} & 0 & 0 & 0 \\ 0 & 0 & 0 & \frac{1}{2G_{vh}} & 0 & 0 \\ 0 & 0 & 0 & 0 & \frac{1}{2G_{vh}} & 0 \\ 0 & 0 & 0 & 0 & 0 & \frac{(1+\nu_{hh})}{E_h} \end{bmatrix} \begin{bmatrix} \delta\sigma_{xx} \\ \delta\sigma_{yy} \\ \delta\sigma_{zz} \\ \delta\sigma_{yz} \\ \delta\sigma_{zx} \\ \delta\sigma_{xy} \end{bmatrix} \tag{2.34}$$

where: ε_{yz} is half of the engineering shear strain γ_{yz} and so on. The stress and strain increments are referred to the rectangular Cartesian axes $x(=h)$, $y(=h)$, and $z(=v)$ with the z axis being vertical. E_v and E_h are the vertical and the horizontal elastic Young's moduli, ν_{vh}, ν_{hh} and ν_{hv} are elastic Poisson's ratios, and G_{vh} is elastic shear modulus. This compliance matrix (Eq. 2.34) is herein assumed to be symmetrical; i.e.

$$\nu_{vh} / E_v = \nu_{hv} / E_h \tag{2.34a}$$

It is usual to assume this symmetry for linear elastic media (i.e., hyper-elastic media). Five individual constants are then left to be determined. It should be noted, however, that there is no theoretical basis for this symmetry for media having stress state-dependent incremental elastic deformation properties (i.e., hypo-elastic media), such as sands.

Under triaxial stress states with the horizontal principal stresses being the same, Eq. 2.34 becomes:

$$\begin{bmatrix} \delta\varepsilon_h \\ \delta\varepsilon_h \\ \delta\varepsilon_v \end{bmatrix} = \begin{bmatrix} 1/E_h & -\nu_{hh}/E_h & \nu_{vh}/E_v \\ -\nu_{hh}/E_h & 1/E_h & -\nu_{vh}/E_v \\ -\nu_{hv}/E_h & -\nu_{hv}/E_h & 1/E_v \end{bmatrix} \begin{bmatrix} \delta\sigma_h \\ \delta\sigma_h \\ \delta\sigma_v \end{bmatrix}$$

(2.35)

In the study by Hoque and Tatsuoka (1998), the shear modulus terms in Eq. 2.34 was not directly considered. That is, elastic shear modulus will not be determined directly from their tests.

Then, elastic parameters were obtained from multiple small-strain amplitude unload and reload cycles (cyclic loading, CL) with a single axial strain-amplitude in the order of 0.001% which was also employed by Kongsukprasert and Tatsuoka (2007). In this strain range, deformation moduli are negligibly influenced by stress-strain histories within the ranges of stress change that are small enough to maintain the initial fabric, the type of loading (monotonic or cyclic), wave form during cyclic loading and the rate of shearing (dynamic or static) (Tatsuoka and Kohata, 1995; Jamiolkowski et al., 1991; Hoque et al., 1996). The two parameters ν_{vh} and E_v were determined from CL tests in the vertical direction at a constant lateral stress (i.e., $\Delta\sigma_h = 0$ and $\Delta\sigma_v \neq 0$) based on Eq. 2.34, we can derive from Eq. 2.35 as:

$$E_v = \Delta\sigma_v / \Delta\varepsilon_v \tag{2.35a}$$

$$\nu_{vh} = -\Delta\varepsilon_h / \Delta\varepsilon_v \tag{2.35b}$$

For horizontal CL tests at a constant vertical stress (i.e., $\Delta\sigma_v = 0$ and $\Delta\sigma_h \neq 0$), Eq. 2.35 shows that:

$$E_h = (1-\nu_{hh})\Delta\sigma_h / \Delta\varepsilon_h \tag{2.35c}$$

$$\Delta\varepsilon_v / \Delta\varepsilon_h = -2\nu_{hv}/(1-\nu_{hh}) \tag{2.35d}$$

It could be seen that the value of E_h cannot be determined only from results of horizontal CL tests without making one assumption. The assumption used in the study by Hoque and Tatsuoka (1998) is that ν_{hh} is constant (ν_1), equal to "ν_{vh} at isotropic stress states". Due to the limited accuracy of the tests, the reliable values of ν_{hv} could not be obtained based on Eq. 2.35d (Hoque et al., 1996).

2.3.1 Inherent anisotropy in the strength and deformation characteristic of geomaterials

Inherent anisotropy in the elastic deformation characteristics is not well understood. Inherent anisotropy is attributed to the depositional process and grain characteristics of the soil mass. Casagrande and Carrilo (1944) defined this type of anisotropy as a physical characteristic inherent in the material and entirely independent of the applied stresses and strains. Besides a strong particle orientation due to deposition, there is also a directional redistribution of particle contacts during shearing. This stress or strain induced anisotropy, which is directly related to particle reorientation, is in particular occurring under stress rotation (Jardine et al., 1986). In most field situations, the sediments have been subjected to some stress history due to geological or other processes and this implies that an in-situ soil is most likely to present a combination of inherent and induced anisotropy. As a result, there is an initial anisotropy, which is one important feature of many natural soils.

The deformation characteristics developed at very small to intermediate strains of a variety of geomaterials are now often evaluated by testing using modern laboratory stress-strain tests. A great amount of such data as above supports the research by Hardin (1978) (e.g., Kohata et al. 1994, 1997, Tatsuoka et al. 1999a, Jiang et al., 1997, Hoque and Tatsuoka, 1998). Based on results from such tests, a hypo-elasticity model with inherent and stress system-induced anisotropy has been developed by extending the research by Hardin (Tatsuoka et al., 1999a, b & c). The major feature of this model is summarized as:

$$E_v = (E_v)_0 \cdot \left(\frac{\sigma_v}{\sigma_0}\right)^m \text{ ; independent of } \sigma_h \tag{2.36}$$

$$E_h = (E_h)_0 \cdot \left(\frac{\sigma_h}{\sigma_0}\right)^m \text{ ; independent of } \sigma_v \tag{2.37}$$

Referring to Eq. 2.36 and 2.37, we have the following relationship between the vertical and horizontal elastic modulus values:

$$\frac{E_v}{E_h} = \frac{(E_v)_0}{(E_h)_0} \cdot \left(\frac{\sigma_v}{\sigma_h}\right)^m \tag{2.38}$$

This equation means that the ratio of $\frac{E_v}{E_h}$ increases in a non linear functions with $\frac{\sigma_v}{\sigma_h}$.

This prediction is support by the data in Fig. 2.9.

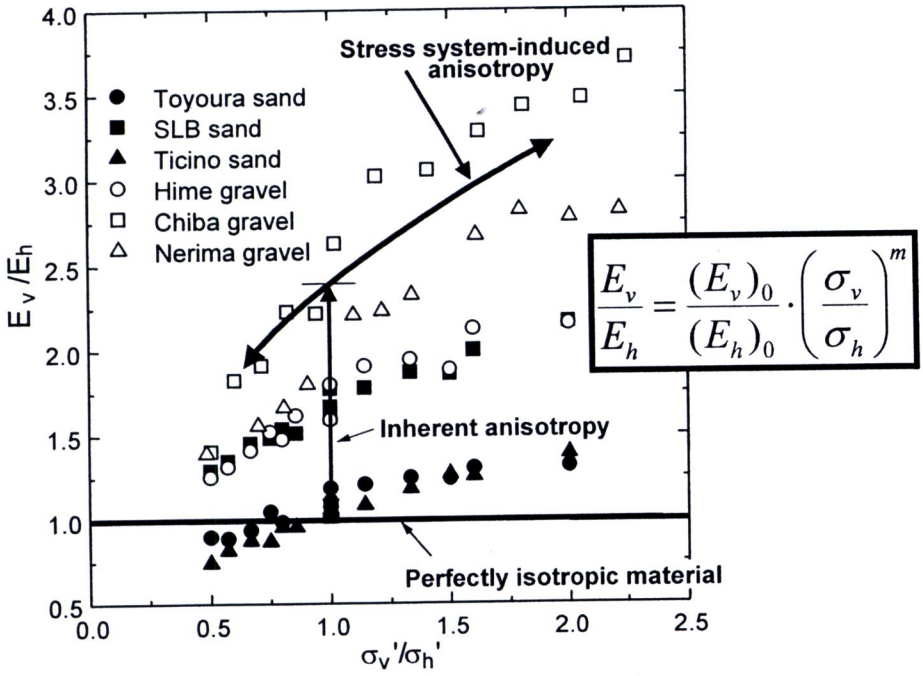

Figure 2.9 Relationships between the ratio of vertical and horizontal elastic Young's modulus values and the principal stress ratio for cross-anisotropic sand and gravels (Kohata et al., 1997, Tatsuoka et al., 1999a)

2.3.2 Compaction-induced anisotropy on geomaterials

Kongsukprasert et al. (2005) investigated anisotropic behavior on cement-mixed gravelly soils. The specimens of cement-mixed gravelly soil were compacted in directions parallel and normal to the direction of axial loading to evaluate the effects of compaction-induced anisotropy on the stress-strain-time behavior of such material. A series of consolidated drained (CD) triaxial compression (TC) test were performed on unsaturated specimens of cement-mixed gravelly soil.

The results show the effects of compaction-induced anisotropy on the stress-strain-time behavior of cement-mixed gravelly soil employed in the study by Kongsukprasert et al. (2005) is not significant at the small strains but becoming more pronounced at larger strains (i.e., at higher stress level). The specimens compacted in the direction normal to the direction of loading may result in reduction of peak strength such that it would become smaller than the one vertically compacted. And, the post-peak stress-strain behavior is rather brittle. The effects of an increase in confining pressure on the stress-strain behavior at small strains are of smaller extent with specimens compacted horizontally than those compacted vertically.

In addition, from other specimens having compaction in the horizontal direction, the shear band seems to always take place in the one specific fashion as illustrated in Fig. 2.10, while shear banding takes place rather more arbitrarily in the case of vertically compaction. It may be inferred that with the specimen compacted in the horizontal direction, since the tensile strength of the lift joint is less than that of the major part of compacted material, as the stress level increases, the weak parts in the lift joints between layers then may start splitting, resulting in a reduction of the peak strength such

that it would become smaller from the one when vertically compacted. In accordance to the aforementioned inference, shear banding always took place in such a same fashion; in such a split like failure mechanism (Fig. 2.10), and with rather brittle stress-strain behavior after peak strength.

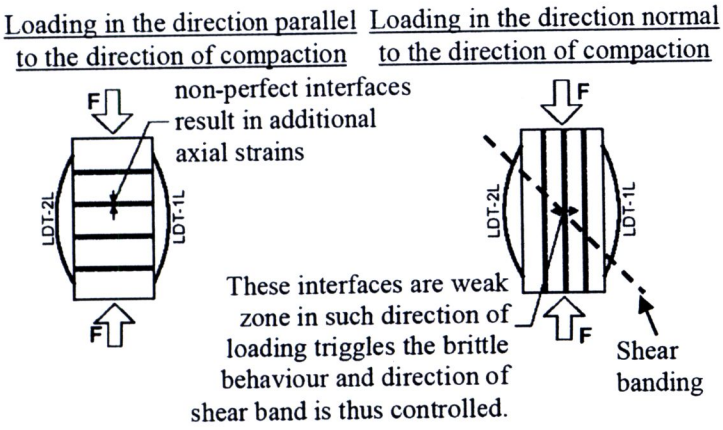

Figure 2.10 Illustrations of two typical directions of compaction (Kongsukprasert et al., 2005)

2.4 Anisotropic behavior of asphaltic concrete

The characterization and modeling of the anisotropic properties of soils have been widely explored in geomechanics and geotechnical engineering. However, very few research studies have focused on the characterization and modeling of the anisotropic properties of the asphalt concrete mixtures. It has been realized that the anisotropy of HMA materials greatly depends on specimen preparation and testing conditions. The behavior is further influenced by the magnitude of stresses and strains induced within the HMA material and the rate of load application. The mechanical behavior of many bound materials such as asphalt concrete mixtures is anisotropic in nature. However, the majority of the current mechanical tests and analytical models for asphalt concrete mixtures are based on the assumption of isotropic material properties. No known pavement structural response model based on layered theory considers the anisotropy of the asphalt concrete materials. Most known models are based on the linear elastic or linear viscoelastic theory. In the linear elastic theory, the asphalt concrete material is assumed to be homogenous, isotropic and linear elastic. The viscoelastic theory considers the time rate of stresses and strains in the asphalt concrete layer, with the similar assumptions of homogeneity and isotropy.

Motola et al. (2006) investigated the degree of anisotropy induced in-situ by the compaction equipment. Three large slabs, about 330 mm × 230 mm were cut from the field. These slabs were sawed in the lab, according to Fig. 2.11, to give nine specimens about 200 mm long, 80 mm wide, and 80 mm thick.

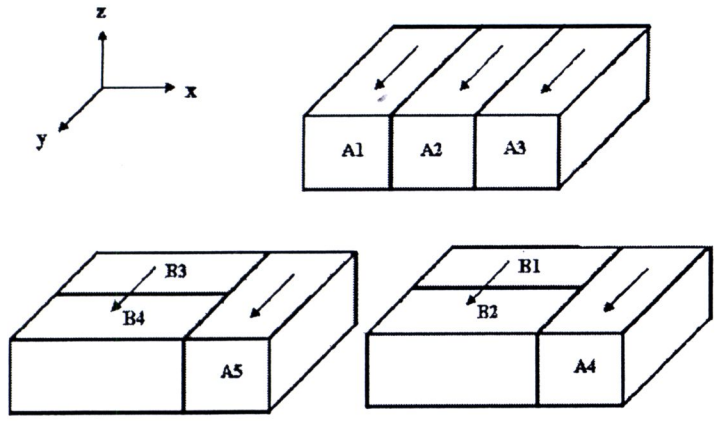

Figure 2.11 Procedure for cutting the specimens

The three principal directions can be tested separately. Every sample was tested in the three directions. Moreover the x and y directions could be tested in two ways, in the long and short dimensions. For example, the y direction was tested in sample A, in the long dimension and in sample B in the short dimension. Since the z direction could be tested only in short dimension, analysis of variance of the results of the x and y directions, and in the long and short dimensions will be used to check the validity of the tests conducted in the short dimension. The specimens were tested in all directions, at 40°C.

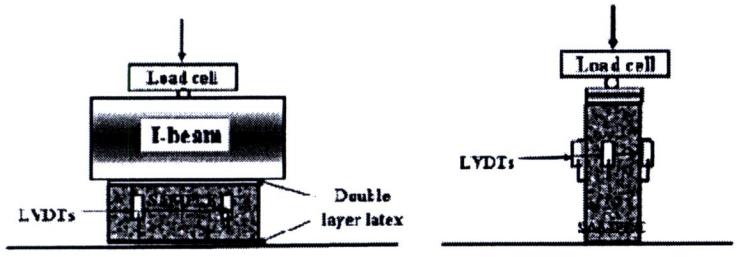

Figure 2.12 Test setup: a) in the short dimension; and b) in the long dimension

From test results, asphaltic concrete material compacted in the field is initially not isotropic, but rather cross anisotropic. The degree of anisotropy is of the order of 40 %. This property should be kept in mind when field samples are tested and/or test results are compared. This is particularly important in uniaxial testing where only one direction is tested.

Wang et al. (2004) performed triaxial laboratory tests on cubical asphalt concrete specimens of 4 inch in lateral length, using a multistage loading procedure. The multistage loading procedure includes isotropic compression (IC) followed by triaxial compression (TC), followed by triaxial extension (TE), followed by simple shear (SS), followed by conventional triaxial compression (CTC), and finally followed by conventional triaxial extension (CTE). Results from the CTC and the CTE tests were used to calculate the magnitudes of the elastic modulus in the vertical direction (E_v) and

in the horizontal direction(E_h). It was found that the vertical elastic modulus was usually two to three times larger than the horizontal elastic modulus. The IC test results showed that the asphalt concrete compacted in the field exhibits anisotropic behavior. The strains induced in the vertical direction were different from those induced in the horizontal directions. They concluded that a larger shear stress may develop in anisotropic materials due to traffic load, thus causing more pronounced shear flow and the accompanied rutting.

Masad et al. (2002) used the aggregate particle orientation as a significant property of the asphalt mixture internal structure to assist in the characterization of the anisotropy of asphalt concrete mixtures. The study showed the significant role played by the aggregate orientation in the characterization of the anisotropic response of the asphalt concrete materials.

2.5 Polymer Modified Asphalt (PMA)

Since the current volume of traffic has increased greatly, the surface of asphalt concrete pavement made by mixture of aggregates and 60-70 penetration grade asphalt cement damage before a reasonable life. These damages include rutting and cracking which cause problems on quality of driving that could lead to serious accidents. Therefore, engineers have tried to solve the problem by using Polymer Modified Asphalt Cement (PM-AC) to replace asphalt cement grade 60/70 (AC-60/70) for mixing with aggregate. The consequence is known as polymer modified asphaltic concrete (PMA). Polymer modification of asphalt emulsions offers improvements in performance and durability, mitigation of pavement distress, and reduced life cycle costs when compared to unmodified asphalt emulsions or hot mix asphalt surface dressings. Polymers have exhibited demonstrable reductions in rutting, thermal cracking, and increased resistance to many forms of traffic-induced stress.

2.5.1 Methods to incorporate polymer into asphalt

Two methods are commonly used to incorporate polymers into asphalt (Becker et al., 2001);

- Addition of latex polymer to the asphalt. This method is relatively easy and trouble free.
- Addition of solid polymers to asphalt. This method normally requires substantial mixing and shearing in order to uniformly disperse the polymers.

2.5.2 Types of Polymer Modifiers

Polymer modifiers are generally separated into two broad categories: elastomers and plastomers (Johnston and King, 2008). A plastomer is a polymer that will deform in a plastic or viscous manner at melt temperatures and becomes hard and stiff at low temperatures; i.e., the structure is reversibly broken down with the application of heat. An example of such a material is ethylene vinyl acetate (EVA). An elastomer is a polymer that has a flexible 'rubber' backbone and large side-chains in its structure. Styrene butadiene styrene (SBS) is an example of this type. Worldwidely, elastomeric polymers comprise approximately 75% of all the asphalt polymer modifiers used. (http://www.bp.com/liveassets/bp_internet/bitumen/bp_bitumen_australia/STAGING/local_assets/downloads_pdfs/pq/pmb_facts.pdf, 2001).

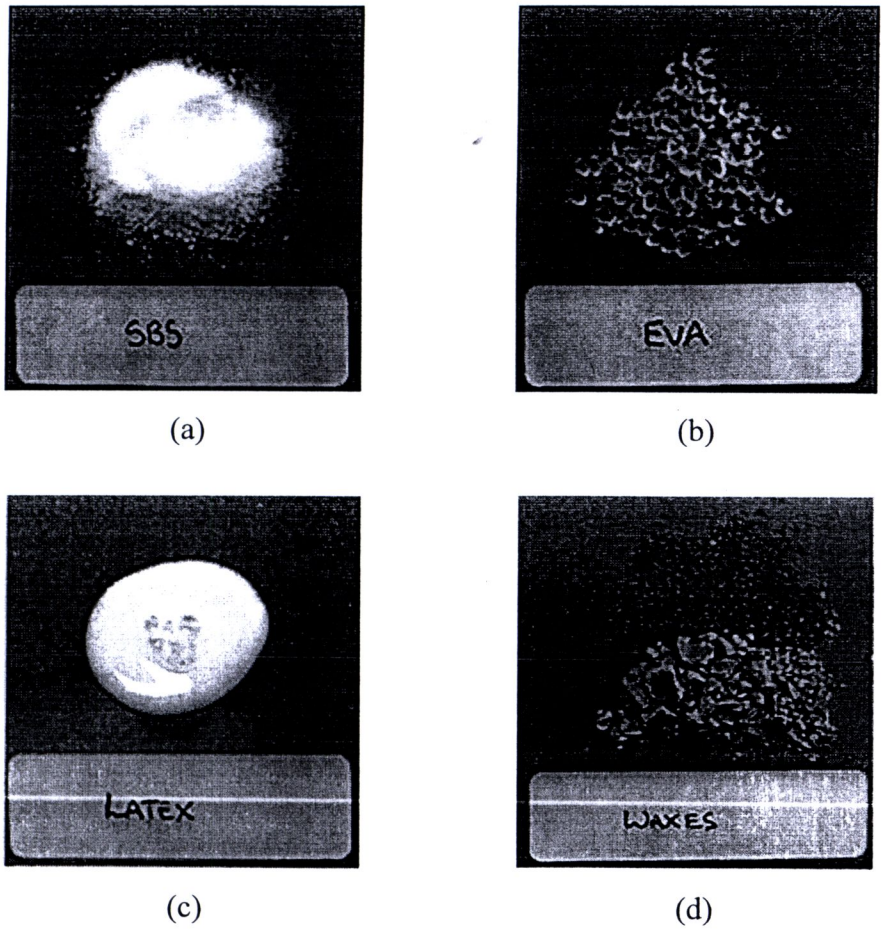

(a) (b)

(c) (d)

Figure 2.13 Examples of different polymers: a) styrene butadiene styrene (SBS); b) ethylene vinyl acetate (EVA); c) latex; and d) waxes (http://www.globalspec.com/reference/50496/203279/chapter-5-polymers-used-in-asphalt, 2011)

Styrene butadiene styrene (SBS) mixtures showed the highest tensile Strength with the Indirect Tensile Test (Fig. 2.14) when comparing with styrene butadiene rubber (SBR) and Ethylene-vinyl-acetate (EVA) (Phromsorn, 1998). So, the most commonly used polymer for bitumen modification is the styrene butadiene styrene (SBS) followed by other polymers such as styrene butadiene rubber (SBR), ethylene vinyl acetate (EVA) and polyethylene (Airey, 2004).

Tayfur et al. (2005) presented a laboratory study of modified bitumen containing styrene–butadiene–styrene (SBS), polialfaolefin (AP), cellulosed fiber (SE), cellulosed fiber mixed with bitumen (BE) and polyolefin (PE). The results indicated that, SBS mixtures shown the highest resistance to the permanent deformation and harmonious results are concern with the repeated creep tests, as shown in Fig. 2.15.

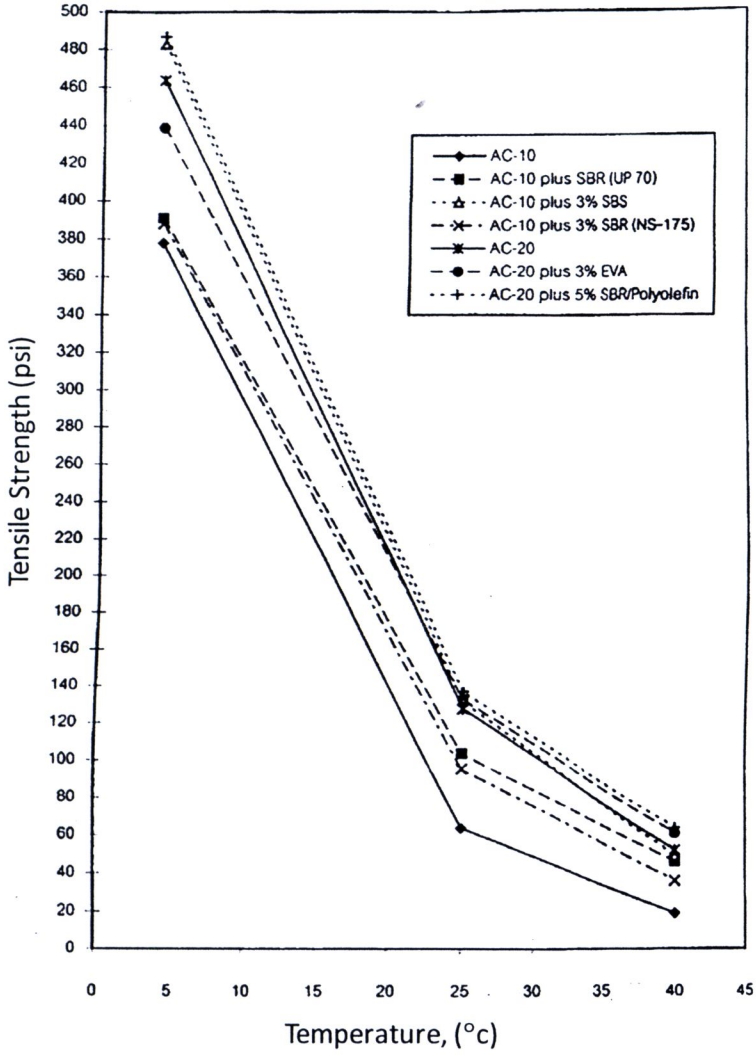

Figure 2.14 Tensile Strength at various temperatures of specimens (Phromsorn, 1998)

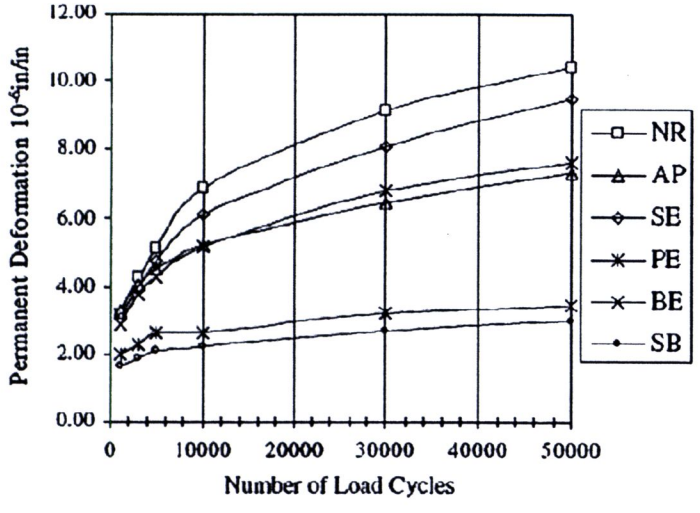

Figure 2.15 LCPC wheel test result (Tayfur et al., 2005)

Lidong et al. (2008) presented effect of polymer on the road application performance of asphalt concrete by mixed specimens of different asphalt and fiber contents. According to the demand suggested in the deformation, wheel tracking tests were performed and the dynamic stabilities and rates of deformation on the specimens. The results indicated that SBS could improve road application performance of asphalt concrete better that other asphalt (Fig. 2.16).

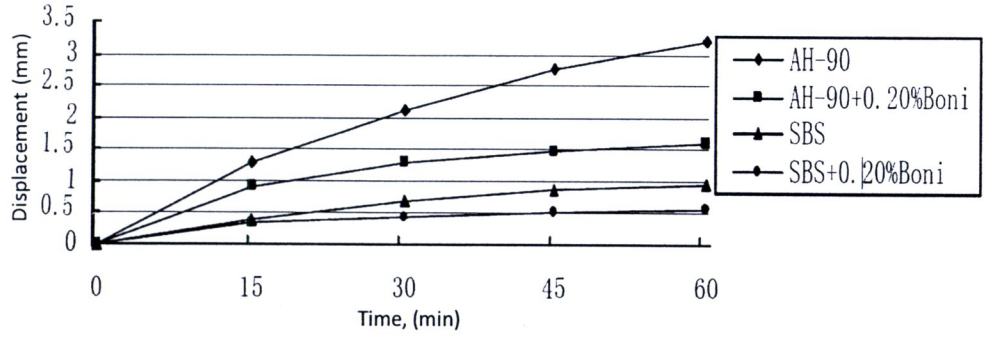

Figure 2.16 Developing process of wheel track (Lidong et al. 2008)

2.5.3 Content of Polymer Modifiers

The (ITS) values increase with increasing polymer content up to 5% as depicted in Fig. 2.17. However, ITS values decrease implying that the increased polymer content at 6%. SBS content does not translate into an increase in the tensile strength of the mixture. So, based on the investigated data, 5% can be accepted as an optimum SBS polymer addition.

The phase morphology of the polymer modified bitumens is the result of the mutual effects of polymer and bitumen and is influenced by polymer content. The formation of a continuous SBS polymer phase is dependent on SBS polymer content. For these particular materials, phase inversion from a continuous bitumen phase to continuous SBS polymer phase occurs when SBS content is around 5%. This content can be accepted as inter-twisted phase which is an ideal microstructure for polymer modified road asphalt, as shown in Fig. 2.18 (Sengoz and Isikyakar, 2007).

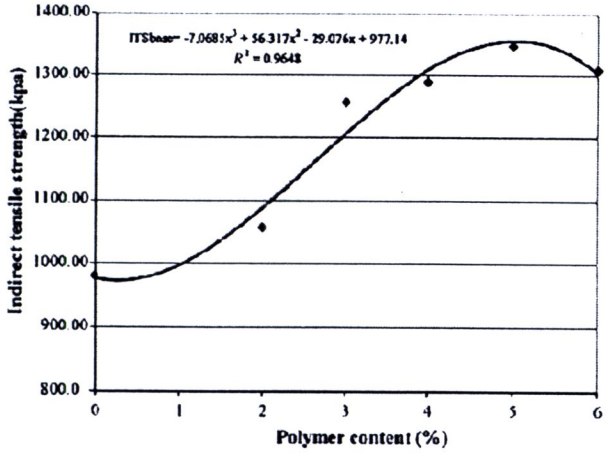

Figure 2.17 Indirect tensile strength values of polymer modified HMA (Sengoz and Isikyakar, 2007)

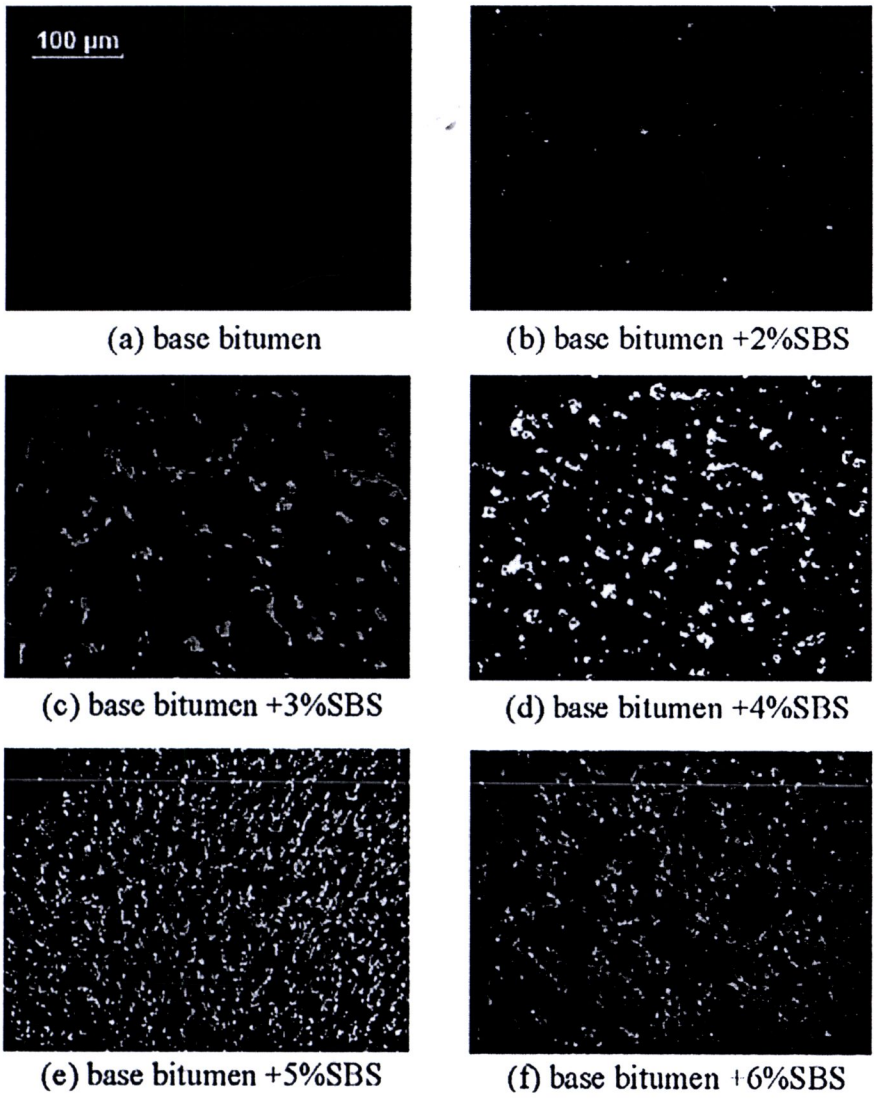

Figure 2.18 Fluorescent images of SBS PMB samples with 100x magnification (Sengoz and Isikyakar, 2007)

2.5.4 Performance of PMA

There are three major damages of road pavement which are generally found and the purpose of modification of asphalt is to reduce such problem. These damages include (Phromsorn, 1998):

- Permanent deformation (rutting)
- Thermal cracking
- Fatigue cracking

2.5.4.1 Permanent deformation Resistance

Polymer modification has been increasingly employed in asphalt concrete, primarily for control of short-term permanent deformation (rutting) (Bouldin and Collins, 1992; Lu and Isacsson, 1999).

Fig. 2.19 presents wet track abrasion losses for 3% SBR, SBS, Neoprene, and NRL modified surfacing treatments in comparison to an unmodified asphalt emulsion. A

mixture modified with 3% SBR can reduce abrasion losses by up to 67% over unmodified asphalt after a 6 day soaking period. Similarly, Neoprene and SBS modifiers improve abrasion losses by 40% to 50%. These results indicate that PME offers significantly increased adhesion (translating into better stone retention) and water resistance than unmodified asphalt emulsions in slurry seal applications. With respect to flushing, Holleran (2006) has shown that loaded wheel test results produce significant improvements in vertical displacement for 3% PME over neat asphalt - particularly for SBR and EVA modified mixtures (Fig. 2.20).

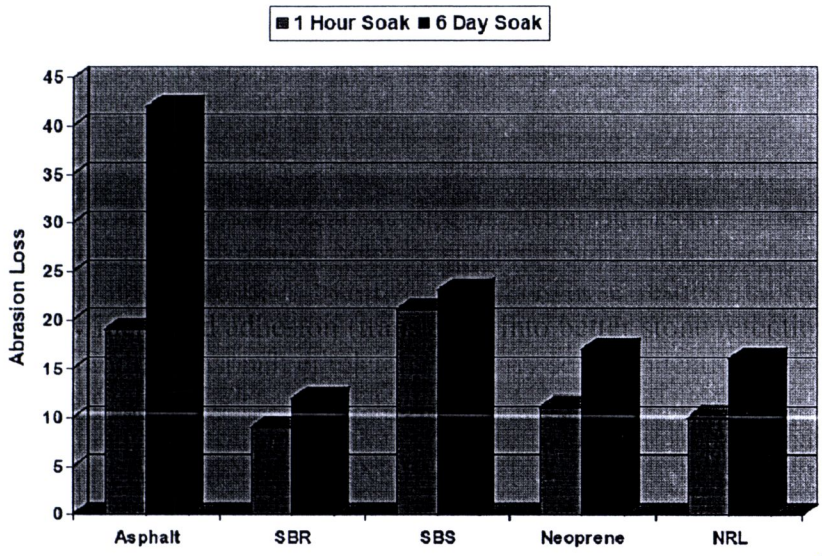

Figure 2.19 Wet Track Abrasion Losses (Holleran, 2006)

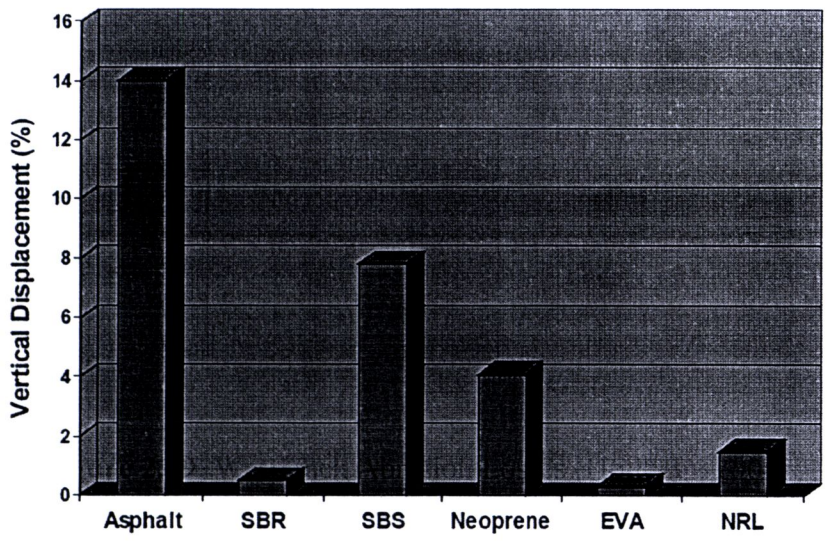

Figure 2.20 Loaded Wheel Test Results (Holleran, 2006)

Chen et al. (2002) reported the development of a procedure to evaluate and optimize a polymer modified asphalt (PMA). Rut depth decreases with increasing polymer percentages, as indicated in Fig. 2.21. The most significant reduction of rutting occurs at the addition of 6% SBS. Adding more than 6% SBS may not be economically feasible, however, because of the limited effect on rutting reduction. Fig. 2.22 shows the tests to study the effect of polymer on the road deformation of asphalt concrete by mixing specimens with different asphalt and fiber contents. The results indicated that the modified asphalt was reduced the deformation more than the unmodified at the same of number of cyclic.

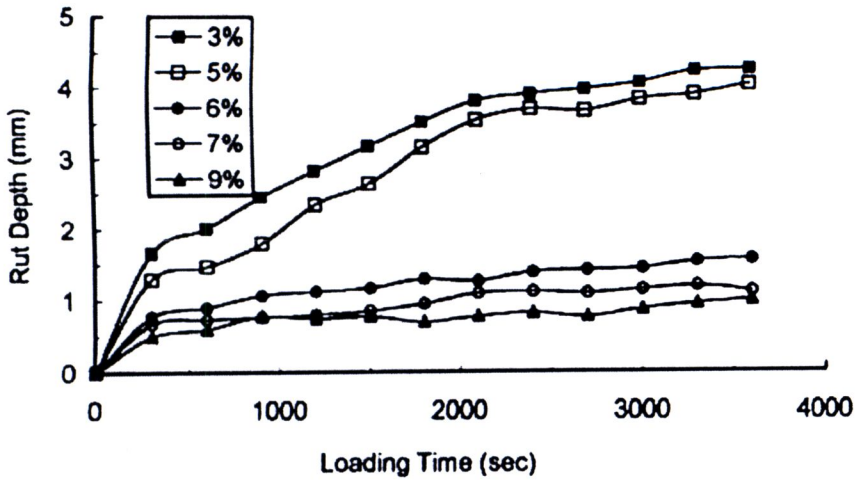

Figure 2.21 Rut depth obtained from the wheel-tracking test (Chen et al., 2002)

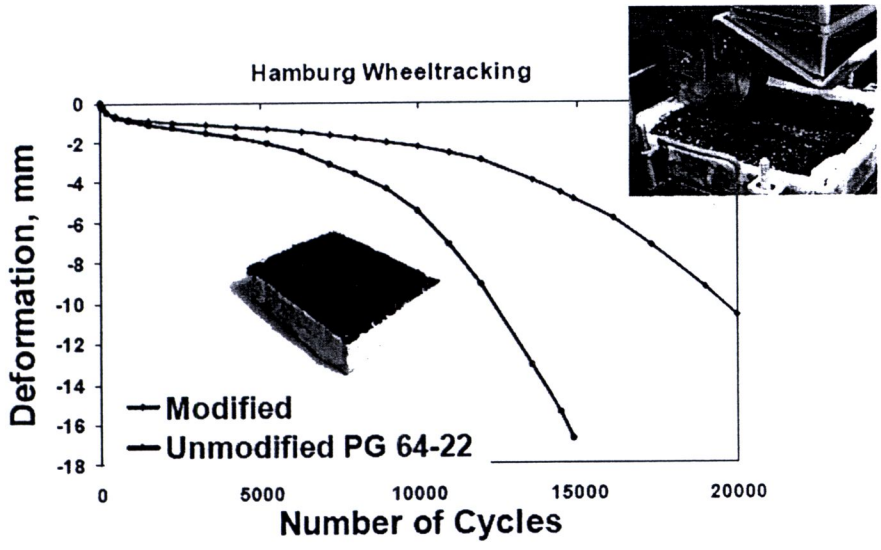

Figure 2.22 Deformation of pavement obtained from the wheel-tracking test (Greater Iowa Asphalt Conference, 2008)

2.5.4.2 Thermal Cracking Resistance

A thermal stress restrained specimen test (TSRST) was performed on polymer-modified asphalt with regard to low temperature behavior (Isacsson and Zeng, 1996). Based on the results obtained, the additions of polymers to bitumens increase the resistance to low-temperature cracking of asphalt pavements.

Low-temperature properties of the modified bitumens containing styrene butadiene styrene (SBS) were investigated using conventional methods, dynamic mechanical analysis (DMA) and bending beam rheometer (BBR). The results indicated that SBS polymers improved low-temperature properties of bitumens. The polymer modification reduces the creep stiffness and limits stiffness temperature of bitumens (Lu et al., 1998).

The lap-shear test was performed to study the interfacial adhesion and behavior between polymer modified asphalts (AC5-SBS and AC10-SBS) and aggregate. At lower temperatures, the lap-shear strength of modified mixtures was higher than those of unmodified mixtures and they increased with increasing polymer (Khattak et al., 2007).

2.5.4.3 Fatigue Cracking Resistance

From investigation of the utilizing a polyester resin for reinforcing flexible pavements, the reinforcement was effective in reducing the stiffness of the mixture whilst improving load-carrying capacity. The effect of the polymer coating was extended to a significant improvement in the resistance to crack propagation, approximately 2.5 times the load cycle of a normal mixture without reinforcement (Kim et al., 1996).

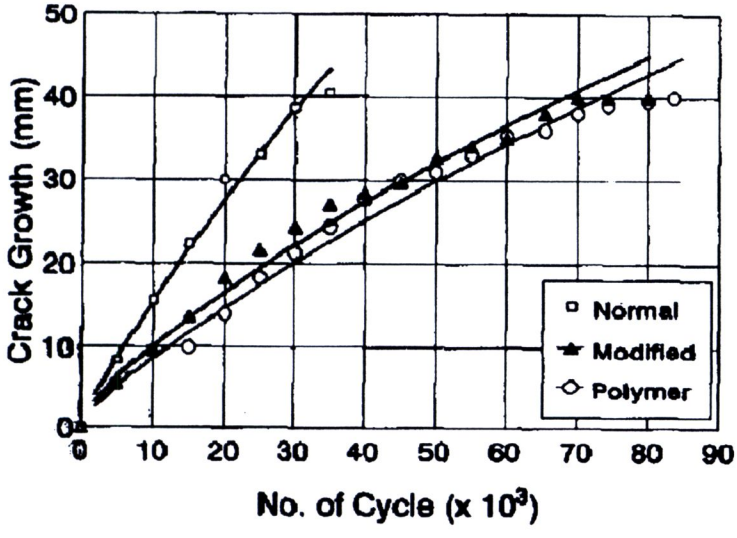

Figure 2.23 Crack propagation by number of load cycles (Kim et al., 1996)

2.6 Anisotropic behavior of Polymer Modified Asphalt (PMA)

Liang et al. (2006) investigated anisotropic behavior of polymer modified asphaltic concrete. Specimens were prepared from the virgin asphalt binder (PG 58-28), and the 5% SBS (Styrene Butadiene Styrene) modified asphalt binder (PG 76-22). After completing the mixing and compaction procedures, the compacted asphalt concrete slab was left for 24 hours in the mold to allow it to cool down to the room temperature. Then, a coring machine with a 4 inches diameter bid was used to extract cores in three orientations: vertical, horizontal and diagonal at 45°. A comprehensive testing program using the repeated triaxial testing procedure is carried out on the specimens with three orientations. The result are shown in Figs. 2.24-2.26.

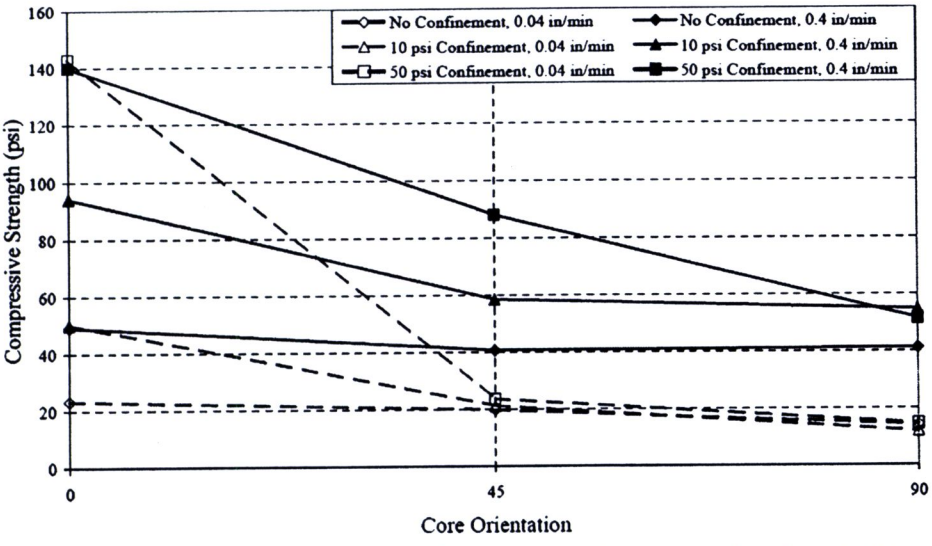

Figure 2.24 Core orientation effects on the compressive strength of asphaltic concrete mixtures containing 5% SBS modified binder (PG 76-22) (Liang et al., 2006)

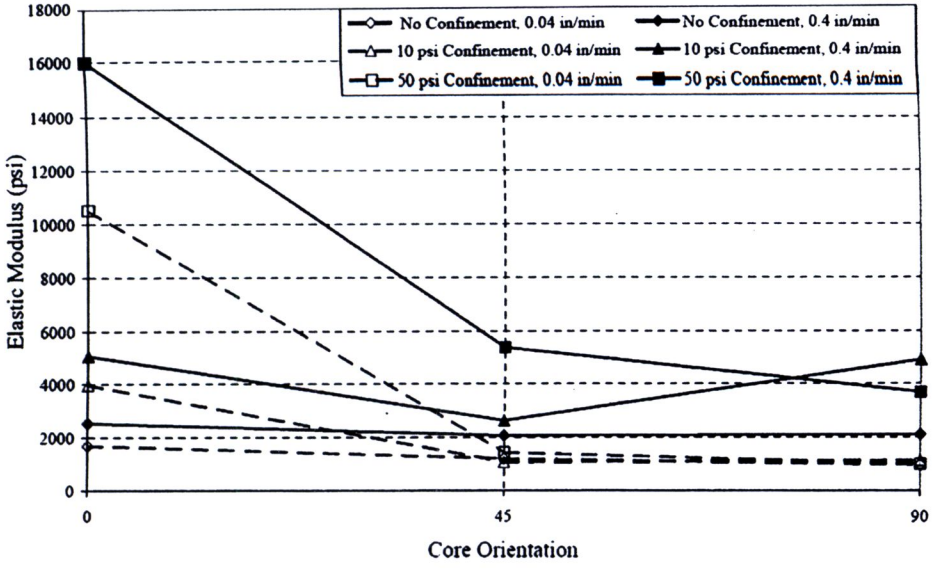

Figure 2.25 Core orientation effects on the modulus of elasticity of asphaltic concrete mixtures containing 5% SBS modified binder (PG 76-22) (Liang et al., 2006)

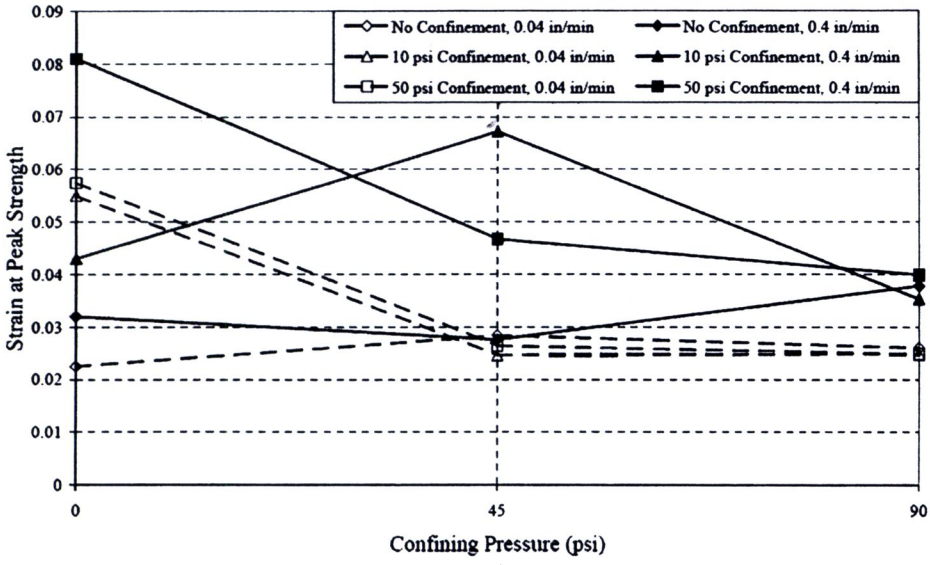

Figure 2.26 Core orientation effect on strains at peak strength of asphalt concrete mixtures containing 5% SBS modified binder (PG 76-22) (Liang et al., 2006)

From test results, both static compression testing and the dynamic testing provided the same observations in terms of anisotropy of the asphalt concrete material. The vertically cored asphalt concrete samples exhibited the highest resistance to the applied loads (both static and dynamic), followed by the specimens cored in the inclined direction, followed by those cored in the horizontal direction. These observations were only true at the low applied axial loads for both types of asphalt concrete mixtures used in both tests. The anisotropic behavior of the asphalt concrete mixtures could be related to the anisotropy in the orientation of the aggregate particles inside the asphalt concrete mix. As a result of the vertical force generated by the compaction process, the aggregate particles embedded in the asphalt concrete mix tend to rotate to the direction parallel to the horizontal direction. This change in the aggregate orientation as a result of the compaction may have resulted in more resistance to the loads applied in the vertical direction due to aggregate interlocking. It could be for the same reasons that the resistance of the asphalt concrete mixtures to the loads applied in the horizontal direction was reduced.

2.7 Basic engineering properties of asphaltic concrete

Asphaltic concrete consists of asphalt binder, aggregates and air voids. The properties of asphaltic concrete depend on the quality of its components, the construction process, and the mix design proportions. In order to be able to produce asphaltic mixtures that have adequate resistance to loading, asphaltic concrete is made by mixing bitumen with aggregate.

Bitumen

Bitumens are hydrocarbons or a visco-elastic material, which are soluble in carbon disulphate. They are usually fairly hard at normal temperatures, but when heated they become soften and flow. Bitumen used in the road construction is asphalt, which is a dark brown to black cementitious material. The asphalt must provide stability, durability, cementation and protection of infiltrating water. Generally, the following

values are used in the classification of bitumens: 1) softening point; 2) ring & ball; and 3) penetration at 25°C. The main physical parameters to describe characteristics of bitumens are: 1) viscosity; 2) shear modulus; and 3) elastic modulus.

Aggregate

Aggregate represents a major portion of asphaltic concrete and it is responsible for the strength and toughness of the material. The physical properties of aggregates significantly affect the performance of asphaltic concrete pavement during its service life. The main properties of aggregates used in bituminous mixtures are: gradation characteristics, hardness, durability, surface roughness, particle shape, and activity.

2.7.1 Components of asphaltic concrete

Asphaltic concrete consists of asphaltic cement, aggregates, and air. However, some asphaltic cement seeps into voids between the aggregate particles, and therefore, is not available to coat and bind aggregates together. This also leaves more air voids in the mixture than would be expected by calculating the total aggregate and asphalt volumes. Figure 2.27 shows the components of an asphaltic concrete. Relative amounts of aggregate, asphaltic cement and air are important (Atkins, 1997).

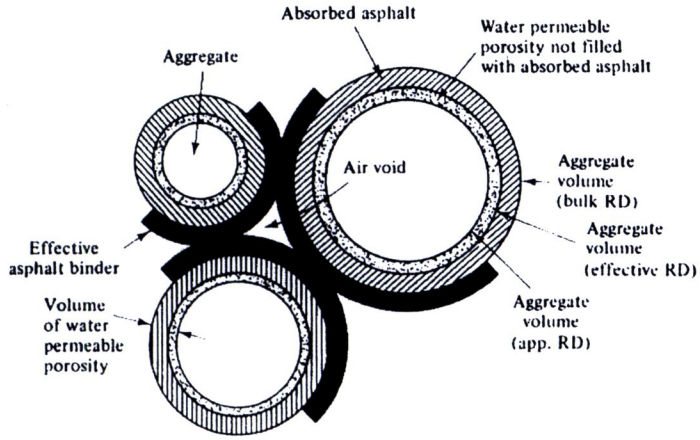

Figure 2.27 Asphalt mixture showing net or effective asphalt, absorbed asphalt, and air voids (Atkins, 1997)

The amount of asphalt absorption is less than the water absorption for the same aggregates, usually by about 50 %. However, it is important to include the volume of absorbed asphalt in calculations, since all volumes must be measured accurately. The amount of asphalt absorption can be found by measuring the relative density of mixture of asphalt-coated aggregates, and comparing this with value expected for with no absorption. The mass/volume relationships of compacted asphalt paving mix are illustrated in Fig. 2.28.

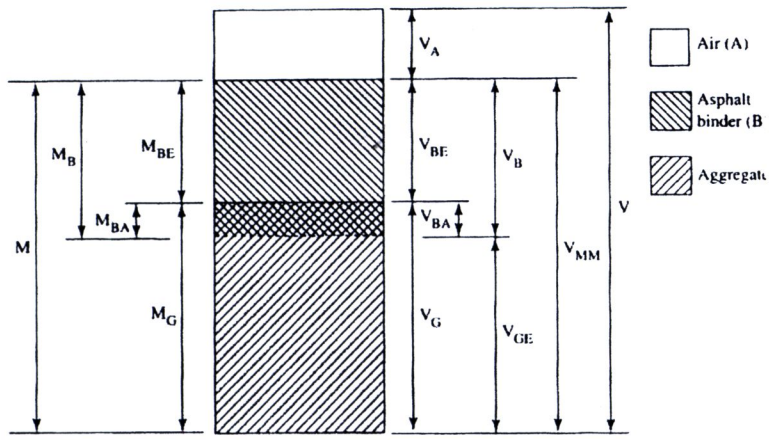

Figure 2.28 Mass/volume relationships in asphalt mixes

where:
M is total mass ($=M_G + M_B$)
M_G is mass of aggregate
M_B is mass of asphalt (binder) ($= M_{BE} + M_{BA}$)
M_{BE} is mass of effective asphalt, the asphalt binder between particles
M_{BA} is mass of absorbed asphalt, absorbed into the pores of the aggregate particles
V is total volume of compacted mix (Assume : $V = 1\ m^3$)
V_G is volume of aggregate, the bulk volume including the aggregate pores
V_{BE} is volume of effective asphalt
V_{BA} is volume of absorbed asphalt
V_B is volume of asphalt ($= V_{BE} + V_{BA}$)
V_A is volume of air between the coated aggregate particles in the mix
V_{GE} is effective volume of aggregate ($= V_G - V_{BA}$)
V_{MM} is volume of void less mix (maximum mix volume)

The bulk volume of the aggregate component of the mix is identified by the symbol V_G in asphalt mixes, instead of V_B (i.e., 'B', in this case, means the 'binder'), to prevent confusion with the symbol for volume of asphalt binder. The bulk volume is usually obtained from the bulk relative density of the aggregate. The effective volume of aggregate, V_{GE}, may be obtained from the effective relative density. Mass/volume relationships usually used in calculation for a mix include:

Density (ρ)	$\rho = M/V$	(2.39)
Asphalt content (P_B)	$P_B = M_B/M$	(2.40)
Effective asphalt content (P_{BE})	$P_{BE} = M_{BE}/M$	(2.41)
Asphalt absorption (P_{BA})	$P_{BA} = M_{BA}/M_G$	(2.42)
Air voids (AV)	$AV = V_A / V$	(2.43)
Voids in mineral aggregate (VMA)	$VMA = (V_{BE} + V_A) / V$	(2.44)
Voids filled with asphalt (VFA)	$VFA = V_{BE} / (V_{BE}+V_A)$	(2.45)

2.7.2 General considerations for preparing asphaltic concrete

Stability of the asphaltic concrete depends on the strength and flexibility of the mixture and the degree of compaction during placing. The strength must be sufficient to carry the load without excessive shear stress occurring between particles. The structure must remain intact. The main contributor for strength is friction between grains. A dense-graded mixture, composes of particles with rough surfaces, with a relatively thin asphalt film between them is best for high-friction strength. Flexibility is also important as the pavement distributes the imposed load by deflecting slightly when the load is applied, without cracking or developing permanent deformation. To meet this requirement, a more open-graded mixture, with a higher asphalt content, is the best. Strength and flexibility are evaluated by various tests, depending on the design method being used.

Safety is very important for the surface course. This involves skid resistance and drainage of water from the surface. Skid resistance is enhanced by using smaller size, very hard aggregates for the surface course. This provides more points of contact for the development of friction forces. In some jurisdictions, open-graded surface courses are used in very heavy traffic areas to allow immediate drainage of rain water before it can result in hydroplaning. These pavements also increase skid resistance due to the coarse texture provided. Open-graded friction courses (OGFC) are not as durable as the usual pavement due to the potential for fairly rapid aging of binder.

Durability of the asphaltic concrete is critical to ensure that it maintains the stability and skid resistance properties for the design service life. Asphalt ages and pavement becomes denser with time and traffic. Pavement fails due to the followings:

- changes in the aggregates
- permanent deformation or rutting
- cracking, either due to fatigue, or low temperatures
- bleeding of asphalt to the surface

To control these failure conditions, the following requirements are usually specified:

1) Use of strong, sound, durable aggregates, free of harmful amounts of deleterious substances. Breakage of particles during transportation, placing, and service reduces strength as there is no asphalt binding the broken pieces together. Traffic could polish soft aggregate particles at the surface, reducing skid resistance. Certain types of aggregate may be susceptible to stripping, or replacement of the asphalt film by water.
2) Use of asphalt binders that are tested for resistance to fatigue cracking, rutting, and low-temperature cracking for the geographic area of use, as required under the new performance-graded specifications.
3) Maximum temperature during mixing to prevent premature hardening of the asphalt as the lighter constituents are driven off.
4) Maximum percentage of air voids to reduce permeability and movement of air and water in the mixture, and therefore reduce the rate of oxidation.
5) Minimum percentage of air voids. This helps to ensure that asphalt does not bleed to the surface and reduce skid resistance. A minimum amount of air allows asphalt movement without forcing it to the surface as the pavement deflects.
6) Minimum percentage of VMA, to ensure that sufficient space is left for asphaltic cement. This helps to ensure that the binder filmed around each particle is thick enough to remain ductile.

7) Minimum and maximum percentages for VFA. Asphalt content must not be too high for light traffic areas, or too low for heavy traffic areas. In general, the controls on VFA ensure that borderline mixtures that meet other void criteria, but may not perform well, are not used.

2.8 Rheology of asphaltic concrete

Rutting in asphaltic concrete layer is caused by densification and shear deformation under repeated axle loads. It develops gradually with increasing number of load applications. Figure 2.29 shows a schematic permanent deformation curve that may be obtained by monitoring road pavements. The initial range, referred to as primary creep range, represents a compaction regime where the material is considered to experience additional compaction under traffic loading. The compaction may result in an improved aggregate interlocking, and consequently, the rut rate (the slope of the permanent deformation curve) decreases. In the second range, known as the secondary creep range, the rate of deformation is slower than during primary creep range and constant. The third range, called the tertiary creep range, is a catastrophic range and is reached when the rut rate begins to increase again. The last range usually involves large scale aggregate movements.

The main attributions of asphalt mixes that can be associated with permanent deformation were discussed by Sousa and Wiessman (1994). These attributions include rate and temperature dependency; dilation; and air-void-dependent behavior. The response of asphaltic concrete is also dependent on loading history and path. Permanent deformation properties of mixtures are also dependent on the binder content and properties of the component materials. Thus, permanent deformation of asphalt mixes is a complex phenomenon of which aggregate, asphalt, and asphalt-aggregate interface properties control the overall performance. This property may change over time as a result of, for instance, aging or moisture damage to the asphalt-aggregate interface. As a result of the influence of the binder, the response of asphalt mixes is dependent on temperature and rate of loading.

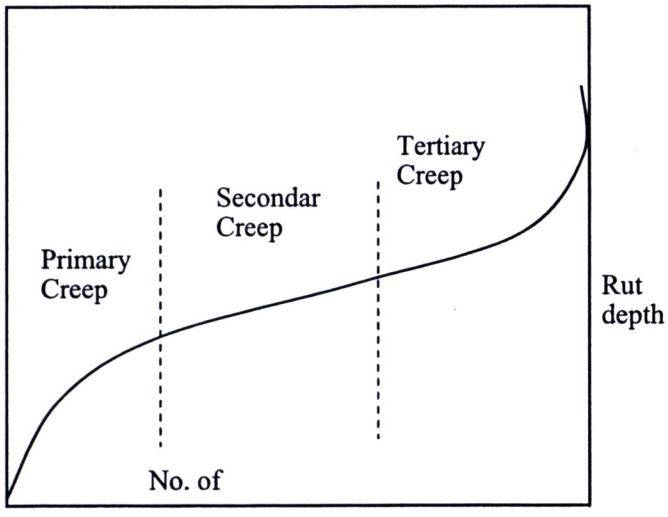

Figure 2.29 Schematic permanent deformation curve (modified from Graba, 2002)

Available evidence indicates that asphalt mixes may dilate when subjected to shearing deformations. This indicates that there is volumetric deviatoric coupling: i.e., deviatoric stresses may lead to volume/pressure change and increasing hydrostatic pressure leads to deviatoric stiffening. Figure 2.30 illustrates the phenomenon of dilation. It shows the results of a study in which specimens having 10 cm in diameter and 5 cm in height were subjected to a sustained shear stress of 35 kPa while the axial stress was maintained at a constant value of 17 kPa (Asphalt Research Program, 1994). It can be seen from the Fig. 2.30 that the rate of dilation is dependent on aggregate structure, resulting from different methods of compaction. It is also indicated from the same study that dilation is dependent on state of stress.

Axial creep tests conducted at different confining pressures provided evidence of stress hardening with confining pressure. Figure 2.31 shows the result of such tests. It can be observed that, with an increase in confining pressure, the permanent deformation was significantly reduced. This is due to an increase of shear moduli resulting from an increase in confining pressure.

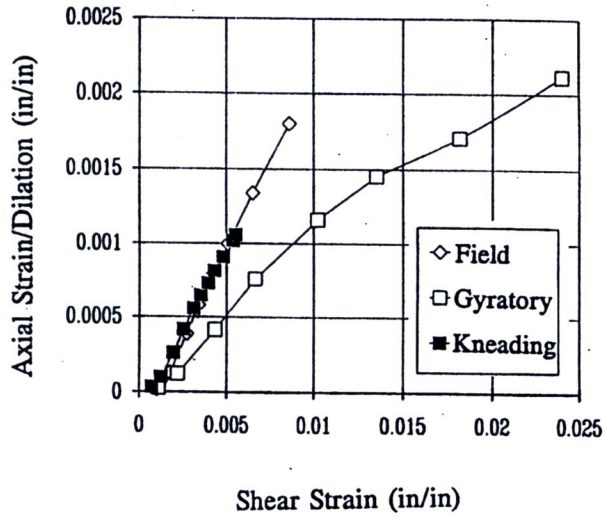

Figure 2.30 Comparative dilational response of asphaltic concrete specimens to shear creep loading (Asphalt Research Program, 1994)

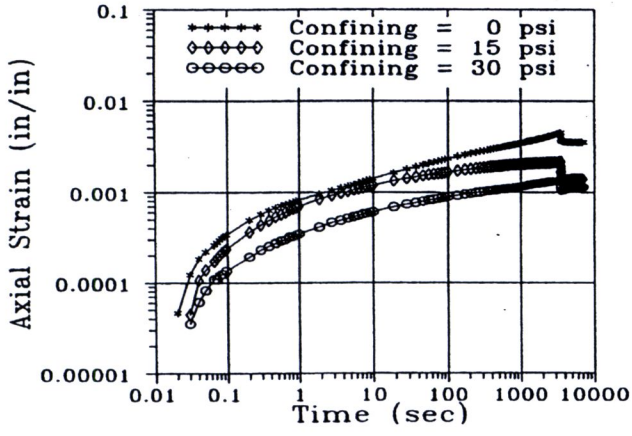

Figure 2.31 Effect of confining pressure on creep behavior at 40 $^{\circ}C$ (Asphalt Research Program, 1994)

2.9 Factors affecting the strength and deformation of asphaltic concrete

In service, asphaltic concrete must provide a stable, safe, and durable road surface. Stability of the asphaltic concrete depends on strength and flexibility of the mixture and the degree of compaction during placing. The strength must be sufficient to carry the load without shear deformation occurring between particles (Garba, 2002). The deformation of asphaltic concrete mixture is a complex process. The binder is time-and temperature-sensitive material. The composite nature of the asphaltic concrete introduces non-linear and stress-sensitive characteristics. Thus, deformation of asphaltic concrete depends on temperature, rate of loading, the state of stress, mix properties, and the volumetric composition (i.e., density, air voids, voids in mineral aggregate, and asphaltic content).

2.10 Laboratory test on asphaltic concrete

The small-strain behavior of soils is great importance in various geotechnical engineering practices where the pre-failure problems are considered. For instance, the predictions of settlements and stress distributions of ground subjected to loadings and excavations demand a proper understanding of the soil stiffness for several orders of strain, say, between 10^{-6} and 10^{-2}. The small strain behavior has also been highlighted in soil dynamics. From specimens, it is crucial to measure local axial strain, of which bedding error is to be excluded in the measurements. The term local strain herein implies a sort of averaged strain determined over a certain length of the soil specimen (Goto et al., 1991).

2.10.1 Uniaxial or unconfined compression test

For a specimen, there are several sources of error involved in the external axial strain measurement, which are:

1) system compliance due to the deflection of load cell, top cap, cell, piston and so on;
2) tilting of the specimen;
3) bedding error on the top and the bottom of the specimen;
4) strain non-uniformity of specimen due to end restraints, leading to bulging of the specimen; and
5) shear banding (strain localization) of the specimen.

Amongst these, shear banding inevitably occurs even when ideal boundary conditions are applied to the soil element. The system compliance can be avoided by monitoring the movement of the top cap of the specimen (Kokusho, 1980). The tilting could also be avoided by using a non-tilting cap. However, in many cases, the bedding error cannot be perfectly avoided in the current configuration of the triaxial specimen. For example, the effect of disturbed zones formed at both ends of the specimen during the sample preparation may be serious for stiff materials in that the observed stiffness would be greatly underestimated. The use of lubrication layers at both ends of the specimen would lead to a low degree of non-uniformity of stresses and strains in the specimen at the expense of increasing the bedding error. Therefore, it is crucial to measure an averaged local strain over the central part of the soil specimen, which is relatively free from the end restraints.

2.10.2 Bedding error

It has been considered that effects of bedding errors at the top and bottom ends of specimen be negligible in triaxial creep tests and unconfined compression tests, considering that they could be significant only when the effective axial stress increases (Tatsuoka et al., 1999b, 2000; Hayano et al., 2001). This is, however, not the case at least with sedimentary soft rock, as shown in Fig. 2.32. In this figure, significant effects of bedding error can be noted as differences in the axial strain between:

a) the external measurement from the axial displacement of the specimen cap detected by means of a proximity transducer (or gap sensor), denoted as AGS (cap), and
b) the local measurement by means of a pair of LDTs, denoted as CLDT, and two pairs of proximity transducers, denoted as BGS (local).

It may be noted that the effects of bedding errors increase not only during monotonic loading stages but also during creep stages. This behavior could be attributed to extra time-dependent deformations of a thin disturbed zone that should have been formed at the specimen ends during specimen preparation. Large differences in the axial strain between the external gauge (denoted as @EXT) and the proximity transducer (denoted as AGS (cap)) is due to the deformation of the triaxial apparatus (i.e., the system compliance). This result indicates that the use of local axial strain gauge is imperative in such triaxial creep tests (Tatuoka, 2000).

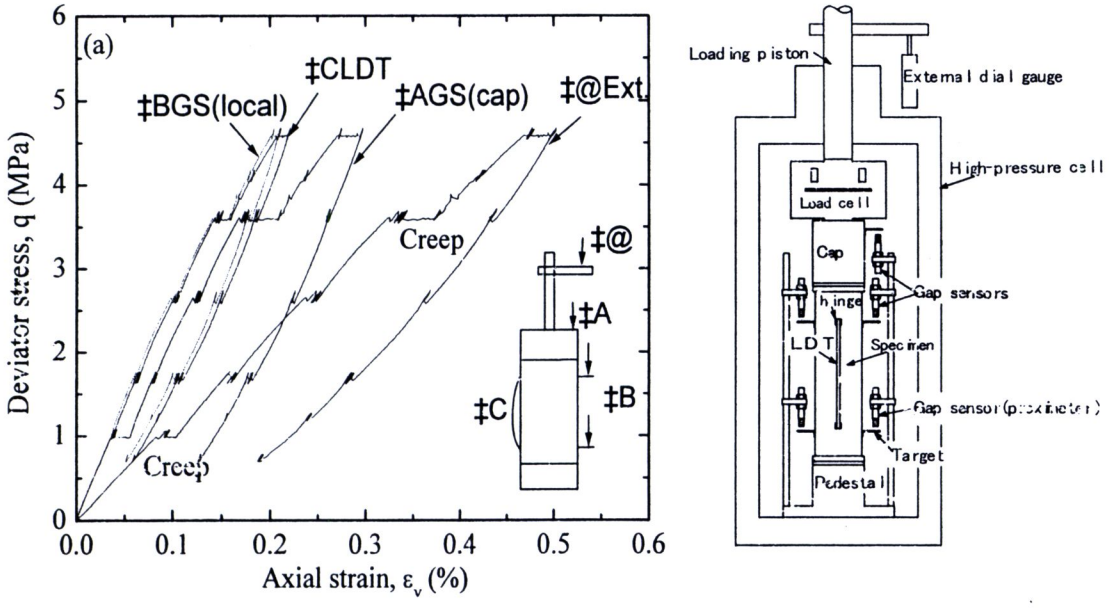

Figure 2.32 Drained triaxial creep test on sedimentary soft mudstone; each creep period is three days (Tatsuoka et al., 1999b,2000; Hayano et al., 2001); the details of the testing method is described in Hayano et al. (1977)

2.11 Void ratio function

A comprehensive series of resonant-column tests to obtain shear modulus at small strain amplitude for round and angular Ottawa sands were performed using solid cylindrical samples by Hardin and Richart (1963). They demonstrated that when the shear strain is below 10^{-3} %, the shear modulus of sand keeps almost constant maximum value. The relationships among shear strain, void ratio (e), confining pressure (p) and maximum shear modulus G (kg/cm^2) are shown by the following:

$$G = 700\frac{(2.17-e)^2}{1+e}p^{0.5} \tag{2.46}$$

Iwasaki and Tatsuoka (1977) obtained that the shear modulus of uniform clean sands without fine soils tested can be represented approximately by the following empirical equations:

$$G = 900\frac{(2.17-e)^2}{1+e}p^{0.40} \quad \text{(at shear strain = } 10^{-6}\text{)} \tag{2.47}$$

$$G = 850\frac{(2.17-e)^2}{1+e}p^{0.44} \quad \text{(at shear strain = } 10^{-5}\text{)} \tag{2.48}$$

$$G = 700\frac{(2.17-e)^2}{1+e}p^{0.50} \quad \text{(at shear strain = } 10^{-4}\text{)} \tag{2.49}$$

Fig. 2.33 shows the relationship between shear modulus for p=1.0 kg/cm^2 and void ratio at different shear strain levels. In obtaining shear modulus for p=1.0 kg/cm^2, measured shear modulus were divided by $p^{0.5}$. Solid curves in Fig. 2.33 represent shear modulus which are proportional to a function $(2.17-e)^2/(1+e)$. It is seen from Fig. 2.33 that the change in shear modulus due to the change in void ratio can be evaluated by the function $(2.17-e)^2/(1+e)$ for wide range of shear strain (10^{-6} to 3×10^{-3}) (Iwasaki et al., 1978).

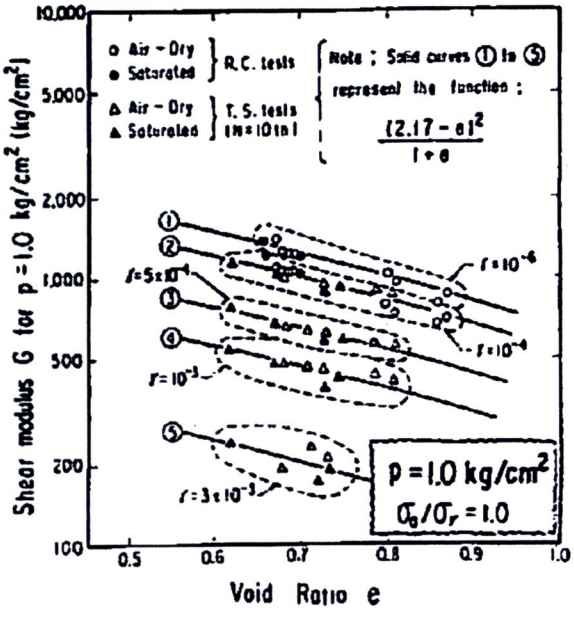

Figure 2.33 Relationships between Shear modulus and Void ratio